Deltares

Enabling Delta Life

Residual dike strength after macro-instability

WTI 2017

Deltares

Residual dike strength after macro-instability

WTI 2017

ir. A. van Hoven

1207811-013

Deltares

Title
Residual dike strength after macro-instability

Client	Project	Reference	Pages
Rijkswaterstaat WVL	1207811-013	1207811-013-HYE-0001-gbh	61

Keywords
residual strength, headcut, erosion clay, wave overtopping, macro-instability, slip failure

Summary
The residual strength of dikes after an initial slip failure was investigated by considering the effect of erosion due to wave overtopping. The negative effect of erosion can be taken into account by an extra margin of 1.5 m of (crest) width for clay dikes, apart from the currently used spatial margins for secondary slip surface failures. The 1.5 m is recommended for existing clay dikes up to 1 l/s/m. For 10 l/s/m the margin for clay dikes increases rapidly (up to 7.9 m) and given the large uncertainties in this study it is not recommended to extend the margin for 10 l/s/m situations. It is recommended not to take into account residual strength for sand dikes overtopped by more than 0.1 l/s/m.

Samenvatting
De reststerkte van dijken na een initiele afschuiving is onderzocht door het effect van erosie door golfoverslag na een afschuiving in rekening te brengen. Voor het opvangen van het effect van erosie moet voor kleidijken bij 1 l/s/m een extra dijkbreedte marge van 1,5 m worden opgeteld, bovenop de gebruikelijke marge. Voor 10 l/s/m kon geen veilige marge worden vastgesteld, omdat de studie teveel onzekerheden bevat. Voor zanddijken wordt het in rekening brengen van reststerkte bij een overslagdebiet groter dan 0,1 l/s/m afgeraden.

Version	Date	Author	Initials	Review	Initials	Approval	Initials
1	dec. 2013	dr.ir. E.J. den Haan		dr. ir. M.A. Van		ir. L. Voogt	
		ing. A.P.C. Rozing					
		ir. A. van Hoven					
2	apr 2014	ir A. van Hoven		dr. ir. M.A. Van		ir. L. Voogt	
		dr.ir. E.J. den Haan					
		ing. A.P.C. Rozing					

State
final

Contents

1 Introduction

Within the WTI2017 program (Dutch Wettelijk Toetsinstrumentarium 2017) research was carried to investigate the residual strength of dikes after an initial slip failure. The WTI2017 program will deliver the statutory safety assessment tools for Dutch primary water defences in 2017. The work was part of the 2013 scope of cluster 5 within the WTI2017 program, which focusses on assessment tools for revetments.

A slip failure does not lead to a dike failure and breaching, if a sufficient part of the dike crest remains intact. This phenomenon is called residual strength, after an initial slip failure. In Dutch practice, the guidelines in the technical report (Technisch Rapport Actuele Sterkte van Dijken) can be followed to determine if a potential slip plane endangers the water retaining function or not. The guideline takes into account the effect of secondary slip failures after the initial one, the secondary failures 'consuming' more dike material. However, the method excludes dikes which have an average overtopping discharge of more than 0.1 l/s/m.

Because many dikes are now designed based on a 1 l/s/m overtopping criterion, giving lower needed crest levels, and due to higher hydraulic loads and higher safety standards dikes tend to encounter more overtopping in safety assessment, there is a need to investigate whether the overtopping criterion of 0.1 l/s/m, when considering residual strength for assessments of existing dikes, can be stretched.

Figure 1.1 Residual dike profiles after wave overtopping induced shallow slip failures after the storm surge disaster of 1953 (Knoeff et al. 2002)

This study focusses on the erosion process after an initial slip failure. Therefor the failure process, in sequence of events and in time, from initial slip failure to breaching of the dike is described (section 2) and the post slip failure geometry is characterized by analysing photos of slip failures (section 3).

In follow up of the Delft Cluster report (Knoeff et al. 2002), the head cut erosion models based on spillway tests in the United States were used to estimate the amount of erosion to be expected (NRCS 1997). Apart from these models, also more recent developments in headcut erosion models are described in this report (Appendix C). These new models are promising because they incorporate the geotechnical stability of the headcut face. Because of practicability, for instance because of the available parameter description and guideline, the conclusive headcut calculations were made using the NRCS models.

In section 4 of the report the hydraulic load by wave overtopping is described. The headcut erosion model is based on tests with a more or less stationary overflow discharge, while in practice overtopping will mainly be -wave-overtopping and not overflow. The hydraulic load is therefore pulsating. The description of the hydraulic load in terms of the distribution of wave overtopping volumes during a storm is based on the EuroTop Manual. Characterisation of the resulting flow conditions on the crest and landward slope were developed within the WTI2017 program. Taking into account the pulsating hydraulic load by wave overtopping is an extension to the earlier work by Knoeff et al. 2002.

Another extension to this work is addressing questions about the applicability of the NRCS headcut models, and suggested parameters, for Dutch situations. A validation was performed for two tests: a wave overtopping test on bare clay at Delfzijl (Figure 1.2) and an overflow test after an initial slip failure at Bergambacht (photo's in section 6). The parameters taken from these post-dictions and the suggested parameters from the NRCS Handbook have led to recommended parameters to calculate the extra crest width margin needed to cope with erosion by wave overtopping after an initial slip failure.

Figure 1.2 Wave overtopping test at Delfzijl where headcut erosion was observed (ComCoast)

This study shows there is a limited and workable extra spatial margin which can be taken into account when assessing the importance of a potential slip surface to cope with erosion after an initial slip failure at 1 l/s/m. For 10 l/s/m the headcut migration can quickly become large, as do the uncertainties about the model outcome.

2 Failure process description

2.1 Introduction

This chapter describes the process of slope instability and possible additional mechanisms leading to a dyke breach, particularly erosion by wave overtopping.

Residual strength after slope instability applies to both inward and outward stability. Although residual strength after an outward slope instability is an issue that needs attention, it is estimated that outward slope instability will not quickly cause a major safety problem. This description covers only the process for the inner slope.

2.2 Description different stages

The process from an initial inner slope slip failure to a dike breach can be divided in subsequent steps and mechanisms:

a. occurrence of an initial slope instability
b. erosion of core material by wave overtopping
c. secondary slope instability of the cliff that remains after the initial instability and (connected to this) micro-instability of saturated dyke material that is exposed after the initial instability
d. dyke breach

The subsequent steps and mechanisms will be described in the following sub-sections. Note that the initial mechanism of a slip failure can also instantly lead to a dike breach if the initial mechanism lowers the crest level below the water level. Subsequent mechanisms b and c are in that case irrelevant.

2.2.1 Initial slope instability, time of occurrence and post slope failure geometry

Due to a high outside water level or otherwise, a slope instability will occur. This can be a more or less circular sliding surface, a sliding surface which is partly circular and partly non circular or even straight due to partly or full uplift of the weak soil layers, or a sliding surface caused by uplift (including blowout) of a thin weak soil layer (where this thin layer loses its strength). Figure 2.1 shows the schematic representations of the different slip failure forms.

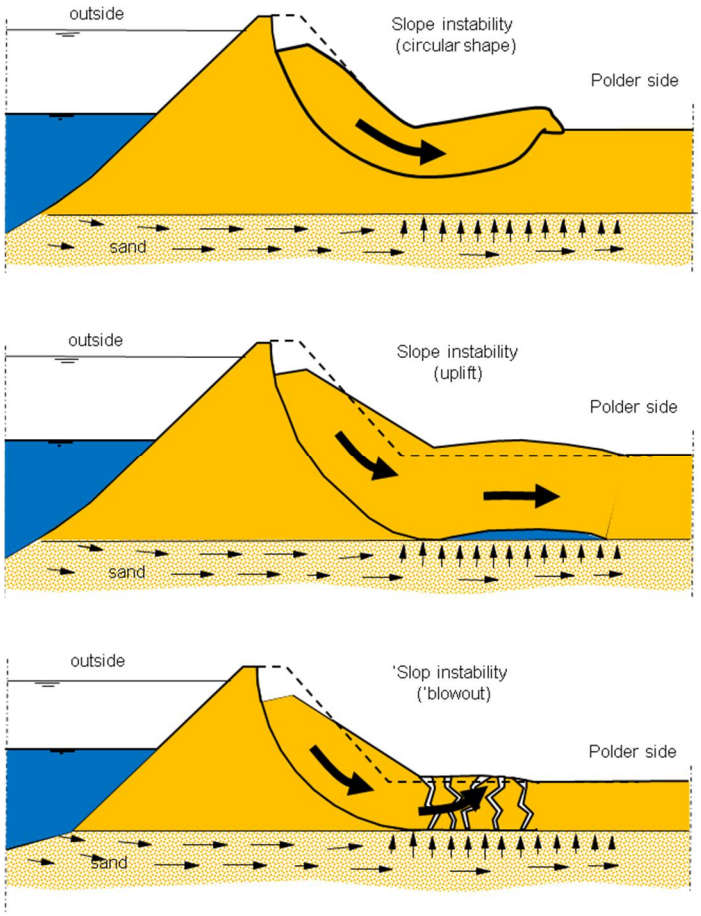

Figure 2.1 Schematic representation of slope instability due to high water levels outside

Time of slip failure occurrence

For the residual strength after an initial slip failure of the inner (polder side) slope it is important to know when the slope failure occurs, or has the highest probability of occurrence. Secondary mechanisms such as erosion due to wave overtopping and micro-instability, ultimately leading to a breach, are time dependent mechanisms. The time between the initial slope failure and sufficient lowering of the outer water level is de critical time where these secondary mechanisms can lead to a dike breach.

The moment of sliding of the inner slope or when the probability of occurrence is the highest, depends on various mechanisms and various loads / processes.

When the load effects (due to high water, precipitation or traffic loads) are high, then the probability of sliding is high. We consider the situation during a high water level. It is assumed that other loads such as traffic loads on the crest of the dyke are present during the normative moment.

A river flood surge caused by heavy rainfall in the river catchment or a storm surge at sea or a lake develops over time. Water pressure against the dyke is highest at the time of occurrence of the maximum outer water level, but determines, only partly, the risk of the inner slope instability. The occurrence of the highest water level and the highest probability of failure do not always coincide. The time between these two events depends on the geo-hydrological response of the dike and subsoil to the high water level and its development in

time. Pore pressures in and underneath the dyke are more important than the water pressure at the outer slope of the dike. The pore pressure depends on the outside water level and permeability of the dyke core and sub soil layers.

For a dyke core and subsoil consisting of permeable sand the geo-hydrological system responds relatively quickly. An increase of the phreatic level in the dyke core due to rising of the outer water level and possibly wave overtopping over the dyke will occur relatively short after the moment of the highest water level. At that moment the (negative) load effect is greatest and hence the risk of slope instability.

For a dyke core and/or subsoil consisting of relatively low permeable clay and peat the geo-hydrological system will respond slowly. An increase of the phreatic level in the dyke core due to the water level against the outer slope and possible wave overtopping will be the highest sometime after the occurrence of the highest water level.

Pore pressures in an aquifer (a water-bearing sand layer under the dyke) react quite rapidly but often the penetration of this water in weak soil layers above the aquifer is delayed. These negative load effects (increase in both phreatic level and ground water head in the sand layer and intrusion in weak soil layers) do not occur simultaneously. At some moment after the occurrence of the highest water level, the (negative) load effect is greatest and hence also the risk of slope instability. For this study, however, it is assumed that the probability of sliding is greatest at the time of the maximum outer water level, which might in some cases be a little on the safe side.

The effect of retardation could take place in more advanced studies, or studies for a specific dike stretch. The tools to incorporate the time effect are available; however, the effect is highly dependable on specific local hydrological circumstances and hydraulic boundaries.

Post slip failure geometry
The uncertainties in the slip surface entry point, in a 2D cross section, have been described in a draft report of the TRMD Technisch Rapport Macrostabiliteit Dijken (in Dutch) (e.g. uncertainty of the location of the entry point of the circle in relation to the calculation model).

Apart from the slip surface entry point, also the lowering of the sliding soil mass relative to the original surface level is important for the following process of erosion which could lead to a breach. As a result of the initial slip failure, a steep and generally a more or less vertical height difference will arise (see section 3 for examples and analyses). In case of a slip failure, the sliding soil section will come to rest as equilibrium is re-established. Sliding will reduce the strength of the (sub) soil along the sliding surface due to large deformations (remoulded strength). A safe approach to this situation for circular slip planes, where uplift does not significantly influence the slope stability, is when (wrongly) no strength along the sliding surface is assumed whereby the initial height difference H, between the upper boundary of the active part (original crest height) and the passive part (original soil level in the polder) is halved. See Figure 2.2 (taken from TAW 1994).

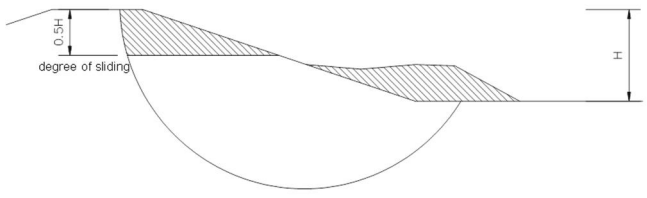

Figure 2.2 Safe assumption of the resulting cross section after initial slope instability

By considering several slope instabilities (section 3), it appears that this assumption is indeed on the safe side. The degree of sliding, and thereby the height difference between the sliding soil section and the original surface level, depends on several factors. One of which is whether or not partly or full uplift occurs. When uplift occurs either a passive slip plane is formed or so-called compression beam is created (cross section in the middle of Figure 2.1). The sub soil in the passive section is (horizontally) compressed and rises. In case of instability due to uplift, it is possible that the degree of sliding, in general, will be larger. Another factor of influence is the remoulded strength of the soil in the slip surface zone.

For this study the 2D- geometry after an initial slip failure will be considered. In reality slip planes will have a limited length along the dike alignment, giving a 3D geometry change when a slip plane occurs. There is no certainty about the length of a slip plane, however, there is to some extent consensus it will typically be in the order of 30-100 m. Based on photographs of slip planes, the deformations near the edges of the slip plane will become less, reducing the initial cliff height near the edges. The lower cliff height reduces the probability of the secondary mechanisms (erosion and/or micro instability) to develop into a breach.

One effect of the 3D slip plane that might increase the probability of erosion after an initial slip plane is concentrated flow along the fissures at the edges of the slip plane. The effect was however not seen at the overtopping test at Bergambacht and the effect is for now not considered. It remains an aspect which might have to be investigated further after this study.

2.2.2 Erosion by wave overtopping

The infiltration of water overtopping the dyke crest and the inner slope (including an inner berm) has a negative effect on the slope stability. Due to infiltration, the phreatic level and the pore pressure increase, resulting in reduction of the effective stress, and thus also the strength of the (sub)soil. This increases the chance of slope instability. For an average overtopping discharge (q) larger than 0.1 l/m/s an increase of the phreatic surface and pore pressures as a result of wave overtopping must be expected.

In case of wave overtopping after initial slip failure erosion may occur as a secondary mechanism (Figure 2.3).

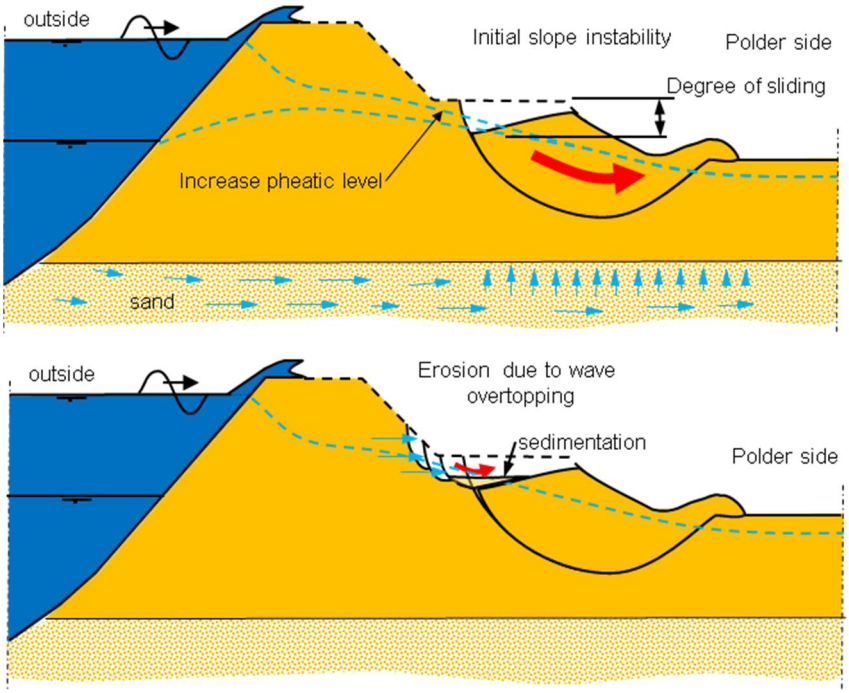

Figure 2.3 Principle of erosion due to wave overtopping after an initial slip failure

The speed of the erosion process depends on the hydraulic load and the material being eroded. For sand directly exposed to overtopping water the erosion process will be relatively fast and only a small amount of residual strength is expected. In cohesive soils the erosion process is much slower and develops in an erosion type called 'headcut erosion'. This type of erosion is described and modelled in section 5 and 6. The residual strength of the dike ends when the cliff migrates to the outer slope and the remaining soil body diminishes below the water level.

If the cliff face intersects the phreatic level in the dike, the cliff migration might increase. This is particularly the case where saturated sand layers or granular road foundations are intersected by the cliff. A combination of the known process 'headcut erosion' and micro-instability of the non-cohesive soil can increase the speed at which the cliff migrates. This effect is not yet addressed quantitatively.

In the current Dutch guidelines an overtopping discharge of 0.1 l/s/m is taken to be a critical discharge below which no significant erosion takes place and above which erosion has to be taken into account.

It is noted that for the Dutch situation it can be stated that erosion, due to extreme rainfall, does not have to be taken into account after initial slope instability has occurred. The combined event of an extreme water level and an extreme rainfall has an extreme low probability of occurrence. For non-Dutch situations this may be different, depending on the rain intensity.

2.2.3 Secondary slope instability and micro-instability

In the current guidelines (ENW 2009, in Dutch) it is assumed that in the remaining soil body after an initial slip failure, a secondary active slip plane may occur further affecting the remaining dike geometry. When determining the residual strength of a dike, the effect of

secondary slip failure is taken into account by assuming a remaining gentler slope, the slope angle of which is determined by the type of soil present.

As a result of micro-instability by outflowing groundwater, the vertical cliff after an initial and secondary slip failure may further erode. In permeable materials such as sand , water will easily flow out, so a more gentle slope can develop. In case of loosely packed sand, the slope is even more gentle. Micro-instability will not occur in homogeneous cohesive soil.
By micro-instability and secondary slope instability, an equilibrium slope may develop of (according to ENW 2009):

- 1:2 for clay with an undrained shear strength c_u (kPa) of at least 3,5* the retaining height (m).
- 1:4 for peat c_u > 3,5* H.
- 1:4 for densely packed sand with ϕ' >22^o.
- 1:7 for loosely packed sand.

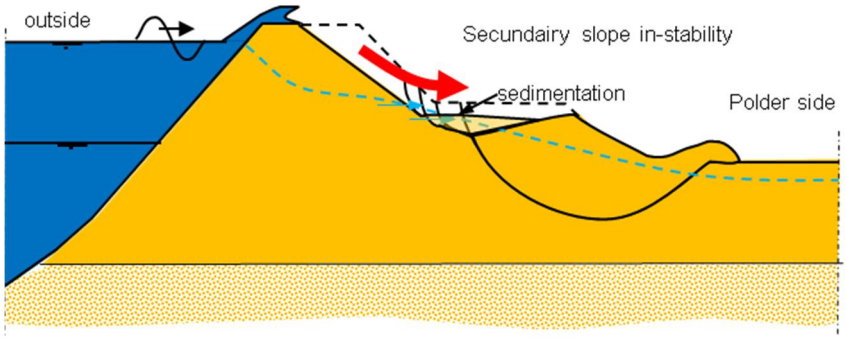

Figure 5: Principle of a secondary slope instability

A clay dike core can be inhomogeneous or layered, where layers or pockets of very permeable materials are present. Examples are:

- Road foundations made of (coarse) granular material.
- Old road foundations later over layered by dike reinforcement, either with new road foundations and a road on top of the old road or with clay.
- Poorly compacted clay layers, where large open pores exist between clay lumps.
- Clay layers with (intensive) soil structure including fissures, which were over layered by later dike reinforcements.
- Sand layers or sand pockets.

These highly permeable layers in a clay core can be susceptible to micro-instability if all of the the following conditions are met:

The base of the permeable layer is lower than the water level.
The permeable layer has a 'permeable' connection to the outer slope.
The permeable layer is intersected by the slip failure

As with 'erosion by wave overtopping' in the previous section it can be stated that if the phreatic level is intersected by the secondary slope instability or cliff erosion, due to permeable materials such as sand or granular material from a road foundation, water can more easily flow out and the risk of a secondary slope instability or cliff erosion can increase.

The effects of micro-instability after an initial slip failure and even secondary slip failure of the remaining soil body is sufficiently covered by the extra soil profile needed given in the current guidelines (TRAS), in case there is no or limited wave overtopping (less than 0.1 l/s/m).

2.2.4 Dyke Breach

The dike breaches if the remaining soil body, after an initial slip failure and subsequent mechanisms (secondary slip failure, micro-instability, erosion by wave overtopping) becomes lower than the water level.

The remaining soil body after initial slope instability represents a residual strength. If there is no significant wave overtopping (less than 0.1 l/s/m) the residual strength must be taken into account according to the current guidelines (TRAS). If there is a significant amount of wave overtopping (more than 0.1 l/s/m) a time dependent erosion process can take place eventually leading to a breach. The erosion mechanism affects the remaining soil body additional to the effects of secondary slip failure and micro-instability.

3 Brief analyses of slip failure cases

In the past a number of slip failures have occurred (paragraph 3.1). The cases were briefly analysed with regard to the post slip geometry (paragraph 3.2).

3.1 Slip failure cases

3.1.1 Sreefkerk

The Streefkerk (South Holland) inner slope failure of the southern Lekdijk, end of october 1984. Length of failure 60 m. The dyke came close to a complete breach. Ironically, the failure occurred shortly after the dyke had been upgraded to meet higher safety standards. The pore pressures due to newly applied overburden on the inner side of the dyke were not fully dissipated when river levels rose and aggravated the situation.

Analysis: Denuded sand appears at the crest where the asphalt road is dissected by the slip. Various near-vertical steps occur with a maximum height of approximately 1m (Figure 3.1).

Figure 3.1 Slip failure Streefkerk

3.1.2 Bergambacht

Bergambacht (51°54'43"N, 4°45'14"E), induced failure of inner slope of a redundant section of the northern Lekdijk, 28 November 2001. Failure by hydraulic uplift of thin, soft polder material at inner toe of the dyke was induced by upstream infiltration of water in the underlying sand layers (approximately 1000 m^3/h at the moment of failure). A basin of approximately 50 m long had been constructed on the upstream side and kept at a high water level to saturate the dyke. Concrete blocks had been placed on the crest, and the ground

surface adjacent to the toe had been lowered (excavated) by 1.5 to 2 m, to further encourage failure. The loss of stability at the toe resulted in the development of a scarp in the crest of 1.0 m high, within 2 hours, and gradually increasing to approximately 1.5 m, horizontal movement at the interface of the deep sand / soft layers (at 12 m - N.A.P.) of 24 cm, and a heave of the polder at the toe of 78 cm at maximum (Figure 3.2).

An induced overflow experiment was performed at this location a few days later, on 5 and 6 December 2001 (Figure 3.3). The source of the overflow was the outside basin, which delivered discharges up to 40 to 60 l/m/s over a section of 12 m in length. An initial breach developed in the outer part of the crest, but its further growth was contained by both the grass cover on the outer slope, as well as by the very hard clay/gravel/asphalt layers below the base of the initial breach, which were very resistant to erosion. After 4 hours of overtopping the depth of erosion of the inner slope was only some 50 cm. It was noted that sand in the crest layers was easily washed away (Delft Cluster 2002).

Figure 3.2 Bergambacht slip failure test

Figure 3.3 Bergambacht overflow test after slip failure test

Figure 3.4 shows the cross section before and after the overtopping experiment.

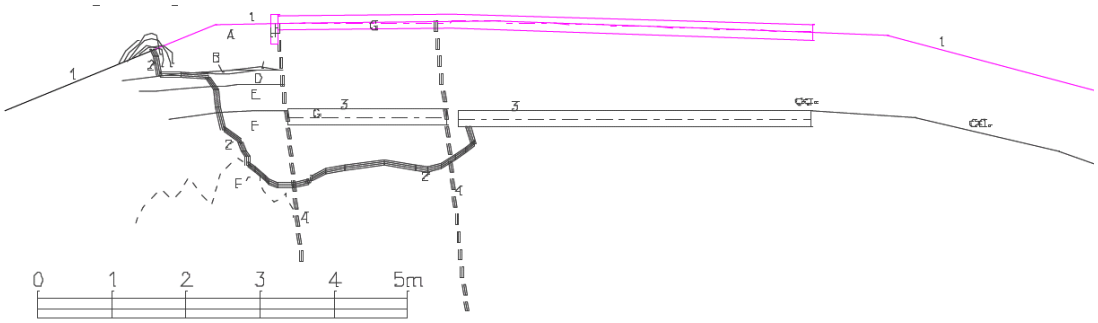

Figure 3.4 Cross section before and after the overflow experiment

1: original dyke
2: schematic of bottom of erosion hole
3: displaced road surface
4: larger slip surfaces

A: sand medium fine
B: asphalt, very local
C: soil + asphalt, local
D: gravelly sand treated with unslaked lime, grey, disintegrated into lumps
E: clay with much gravel, mostly in layers, coarse prismatic structure, few wormholes

F: clay, medium silty, brown, coarse prismatic structure, many wormholes, locally many very fine holes
F': clay, medium silty, grey (reduced), little structure
G: asphalt and sub coarse
H: concrete containing band, often displaced / removed

3.1.3 Polder Beschoot

Polder Beschoot (North Holland) canal dyke, failure of inner slope along inner verge of asphalt road on shoulder (berm)

Analysis: Cause of failure unknown, but probably not associated with high outside water levels. Vertical step in road base material less than 1 m high.

Figure 3.5 Polder Beschoot canal dike

3.1.4 Nieuwe Zuider Lingedijk

Nieuwe Zuider Lingedijk, Heukelum (South Holland). This is a dormant, dry dyke, in place as a second line of defence. The failure is therefore not hydraulically induced. The asphalt crest road is cracked along the centerline, revealing a subvertical face of about 40 cm of asphalt.

Figure 3.6 Nieuwe Zuider Lingedijk

3.1.5 Oude schild Texel

Sea dyke inner slope failure, Prins Hendrikdijk, Oude Schild, Texel. Analysis: Cause unknown. Slump of inner slope, with a steep scarp of denuded clay, height approximately 50 cm.

Figure 3.7 Oude Schild sea dike Texel

3.1.6 Schipluiden

Schipluiden (South Holland), former tramway embankment. Near failure after flooding a new marina constructed adjacent to the embankment. The marina connects to a canal standing 3.5 m proud of the polder. The embankment was not designed as a water-retaining structure, and leakage through it started quickly after breaching the canal dyke at the marina.

Analysis: The down stream slope slumped along the asphalt road verge, where a sub-vertical step of about 1 m high developed. Total slope height at the slip is approximately 3 m. The scarp curved away from the road verge to both sides of the slipping mass.

Figure 3.8 Schipluiden

3.1.7 Het Bildt

Het Bildt (Friesland), slips in inner slope of Oudebildtdijk. Vertical scarps approximately 50 cm high.

Figure 3.9 Oudebildtdijk

3.1.8 Wilhelminakanaal

Wilhelminakanaal (Noord Brabant). Vertical scarps approximately 40 cm high in canal dijk.

Figure 3.10 Wilhelminakanaal

3.1.9 Steinse dijk, Haastrecht

Steinse dijk, Haastrecht (South Holland). Vertical, 1.5 m high scarps in slumped inner slope of Hollandsche IJssel river

Figure 3.11 Steinse dijk, Haastrecht

3.1.10 Zuider Lingedijk, Spijk

Zuider Lingedijk, Spijk (South Holland, 51°51'29"N, 5°01'33"E) Slump starting halfway down inner slope. Clay, high 1 m.

Figure 3.12 Zuider Lingedijk, Spijk

3.2 Overall analysis of picture material

Most of the cases show a steep scarp of limited height (40 - 100 cm, representing 20 - 40% of dyke height) at the head of the slip. The slips often develop along the road verge and cut through road base material which is often sand and other granular material. In a minority of cases the slumps start approximately at midheight in the slope.

It should be noted that the inner slope failures generally did not develop as a result of high outside water levels, and certainty that the cases are representative of the problem at hand, inner slope failure due to high outside water levels, is absent. However, it is considered unlikely that the shape of the slips will be very different from those presented by the photo material, when high outside water levels form the main loading, and so for the present analyses, we will apply the indications from the picture material and assume that near vertical scarps of limited height will develop at the head of the determining slip plane.

The cracks and fissures which accompany the scarps presented in the photo material, will possibly allow concentration of flow during overtopping, which could aggravate the rate of erosion. Many of the cases shown however present the scarp as a clean initial failure surface, and in those cases it is unlikely that water will emanate from within the dyke onto the scarp and increase flow. The matter is different in the cases where the inner slope fails high up the slope and multiple cracks, fissures and terraces are formed in the crest. Then it is likely that the cracks will concentrate the flow and that erosion will be strongest around the cracks. Note however, that in the case of the Bergambacht overtopping experiment, where such cracks occurred, overflowing nevertheless did not lead to heavy erosion. In summary, there is no indication that concentrated flow in cracks and fissures merits special research.

An obvious consequence of the near vertical scarps which form on the inner slope after a slip, is that the slope angle itself is not the determining factor with regard to the erosion and cliff. The erosion from the very beginning occurs on a steep, sometimes vertical, bare face.

4 Characterization of the wave overtopping load

4.1 Introduction

Erosion of the dike after a slip failure is caused by the wave over topping discharge. The over topping discharge is highly pulsating. Within the WTI2017 framework, cluster 5 revetments, much knowledge was gathered on the characterisation of this pulsating erosive load by wave overtopping. In this section the load is described for use in section 5 and 6 where the load is used as input for the head cut erosion models. The knowledge on the wave overtopping load was developed for the use in grass-erosion models, which uses the maximum flow velocity instead of the discharge which is used in the head cut erosion models.

The erosion calculations require a representation of the discharge flowing over the dyke crest and landward slope as a result of wave overtopping. In engineering practice the average discharge q_a ($m^3/s/m' = m^2/s$ or commonly used l/s/m') during a storm is often used. In Dutch dyke practice q_a is often in the order of 0.1 to 10 l/s/m' in design conditions. However, during a storm the overtopping discharge will consist of multiple overtopping waves. Because the waves in a wave field are irregular the overtopping wave volumes are also irregular. The total overtopping volume during a storm, q_a*stormduration, will consist of a range of individual overtopping volumes ranging from small to large.

4.2 Load duration

A slip failure of the inner slope is most likely to occur during the presence of a high water level, or shortly afterward. An assumption on the safe side is that the slip failure occurs before or at the start of the wave overtopping event. The duration of a wave overtopping is in the order of several hours, for sea, lake and river dykes alike. An estimated duration of the peak overtopping load of 6 hours is on the safe side. The peak load will only occur during the peak of a storm. On the flanks of the storm surge the overtopping load will be less severe.

4.3 Load characterization in terms of individual overtopping wave volumes

The report 'Technisch Rapport Golfoploop en Golfoverslag bij Dijken' (TAW 2002), gives a method to calculate the number of waves from a wave field overtopping the dyke crest (N) and the distribution of water volumes V (m^3) overtopping a dyke as a function of a dyke geometry, water level and wave conditions.

For the present study three different wave climates will be taken into consideration characterised by a wave height H_{m0} = 2 m, (sea, lake and estuary dykes), H_{m0} = 1 m (lakes and rivers in the tidal zone), H_{m0} = 0,5 m (rivers). Two different average wave overtopping discharges will be considered, 1 and 10 litres per second per meter (l/s/m)

An overtopping wave volume V_i (volume number i, where i ranges from 1 to N) generates a velocity u_i (m/s) and water layer thickness h_i (m) profile which can be approached by a triangle when plotted against time t (s).

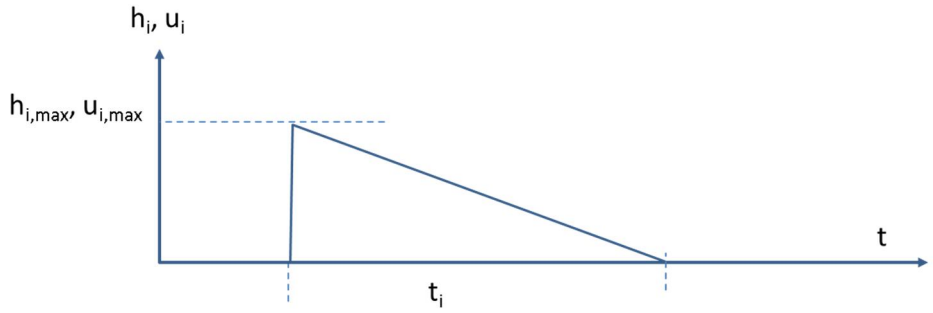

At the front of the overtopping volume, the depth averaged velocity and the water layer thickness are maximal, after which the decrease linearly to zero. The discharge q at a certain spot on the dyke crest and inner slope is equal to h(t)*u(t), resulting in a parabolic q-profile against time.

From the WTI 2017 research empirical formulae are available to estimate the maximum velocity and water layer thickness of a wave volume on the dike crest:

$$h_{i,max} = 0.133 V_i^{0,5} \quad (4.1)$$

$$u_{i,max} = 5.0 V_i^{0,34} \quad (4.2)$$

Resulting in the formula for the maximal discharge:

$$q_{i,max} = 0.665 V_i^{0,84} \quad (4.3)$$

The time t_i (s) it takes for a wave overtopping volume V_i ($m^3/s/m'$) to pass a certain point on the crest or inner slope can be calculated by integrating q from t = 0 to t = t_i:

$$q_i = h_i \times u_i = h_{i,max} (1 - t/t_i) \times u_{i,max} (1 - t/t_i) = q_{i,max} (1 - t/t_i)^2 \quad (4.4)$$

$$V_i = \int_0^{t_i} q_{i,\max} (1 - t/t_i)^2 \, dt = \frac{1}{3} q_{i,\max} t_i \quad (4.5)$$

giving $t_i = 3 V_i / 0.665 V_i^{0.84} = 4.5 V_i^{0.16}$ (4.6)

With the empirical formulae the irregular overtopping discharge during a storm event can be described. For example consider a 6 hours storm with an average wave overtopping discharge of 1 l/s/m and a wave field characterized by a significant wave height H_s=1 m, a peak period T_p=4 s and a mean wave period $T_m=T_p/1.265$= 3.16 s. There will be approximately 6800 waves reaching the dyke within the storm period, with an overtopping probability P_{OV}=0.072 (TAW 2002) leading to ca. 500 overtopping events. The water volumes per overtopping event can be approximated by a Rayleigh distribution. The volumes are represented in Figure 4.1, ordered from largest to smallest.

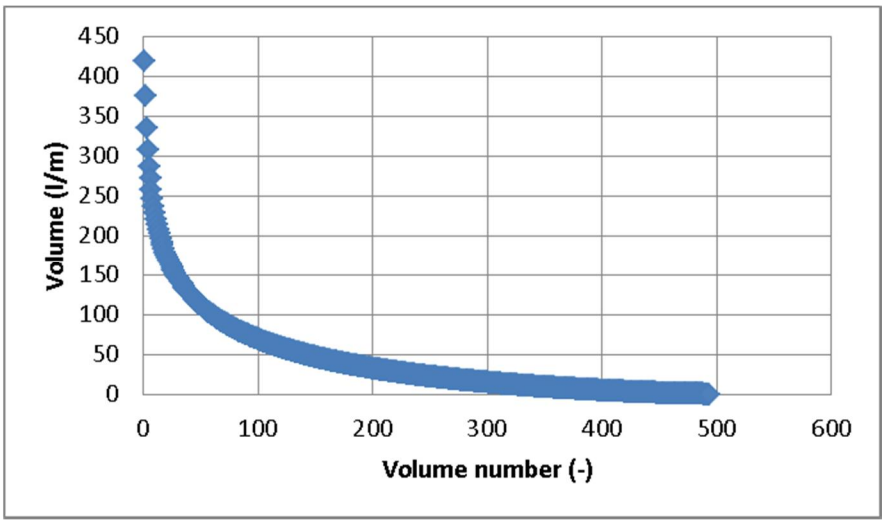

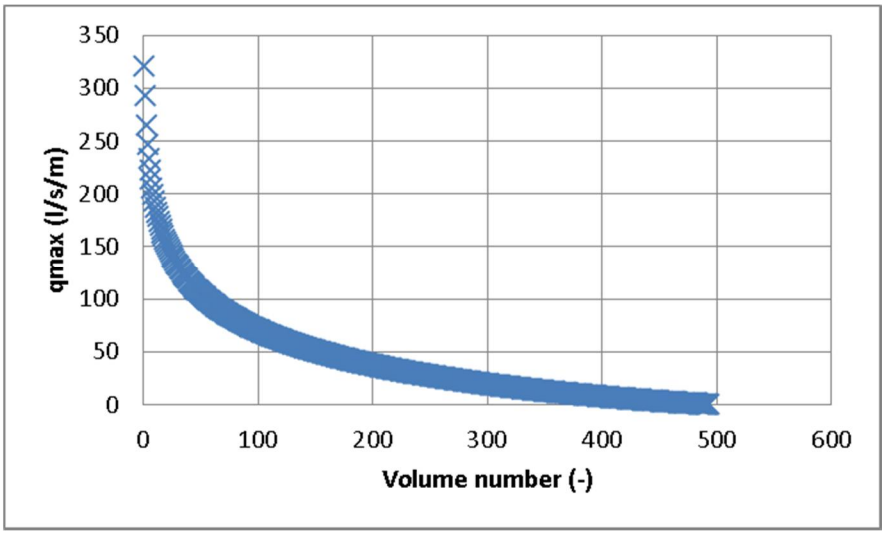

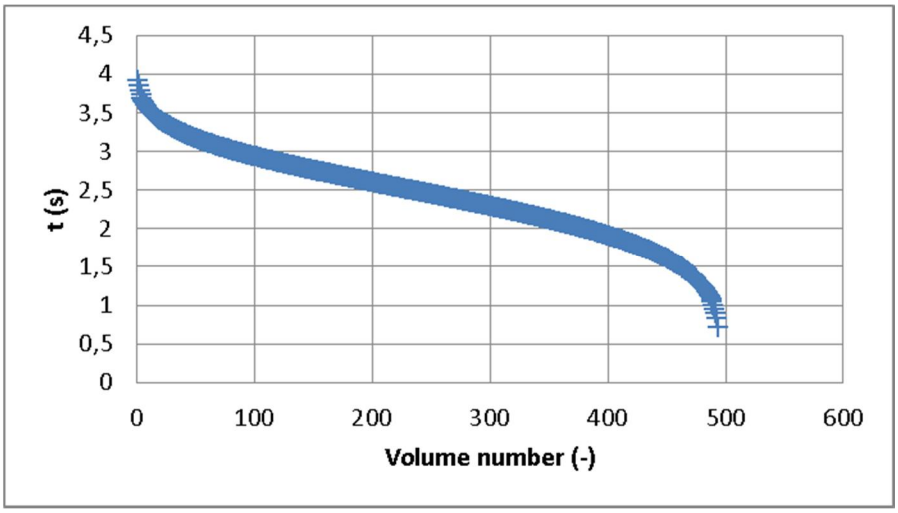

Figure 4.1 Overtopping wave volume (l/m), q_{max} (l/s/m) and period of overtopping volume (s) for each of the approximately 500 overtopping events in a 6 hour storm condition with Hs = 1 m; q=1 l/s/m

The sum of all overtopping times t is 1200 s, or approximately 20 minutes (5.5% of storm duration). During the 6 hours storm only a limited amount of time there is a significant discharge flowing over the dyke crest and slope. The average discharge during the 1200 seconds is 18 l/s. It has to be noted however, that the slope of the dyke will have a very thin water layer on top of the slope much longer than 1200 s. According to the Handreiking Toetsen Grasbekledingen (MinIenM 2012), a thin water layer will be present approximately 70% of the storm duration (4h 12 min). This is an approximation of the time used for infiltration calculations, where even a very thin water layer in between the grass sod, will still provide water for infiltration. When considering erosion this small water layer is not relevant, because the flow velocity will be below the critical velocity of dyke materials.

4.4 Load cases for further erosion analyses

Three different storm cases and two different average overtopping discharges will be studied for their effect on headcut advance in section 5 and 6. Each has a duration of 6 hours, an average discharge over the 6 hour period of either 1 or 10 l/m/s, and wave heights which are characterised by H_s = 0.5, 1 and 2 m, and a wave steepness s_{0p} of 0.04, based on the peak wave period and deep water wave length. These discrete storm conditions represent a wide range of cases in The Netherlands. Higher waves and/ or overtopping discharges can occur, but are rare. The characterisation of the selected cases is given in Table 6.6 and Table 6.8.

Note: Concentrated flow- off through fissures is for now discarded and the 2D situation is considered. See also section 3.2.

5 Rapidity and quantification of erosion

5.1 Introduction

The analyses of picture material of inner dyke slope failures showed that most slip planes develop through the crest (road) or along the landward road verge (Section 3). A minority of slip planes occur approximately halfway the inner slope. For the purposes of erosion analyses, both cases present an already formed scarp which will quickly take on the function of a headcut once overtopping gets underway. The method of analysis adopted in this report is to consider the scarp as a pre-formed headcut, the advance of which towards the crest due to overtopping erosion is to be calculated.

The crest slip planes are characterised by a horizontal approach surface above the scarp. This resembles the case of the free overfall. The materials involved will be grass or asphalt above the overfall, usually unbonded or bonded granular material in the scarp, and asphalt, grass or granular material beneath the plunge pool. Obviously, where unbonded sandy material appears it is not likely that any erosion resistance of importance can be counted on.

For slip planes starting on the grass slope, the approaching water along the inner slope has gained (or lost) a velocity determined by slope inclination, roughness and discharge. Velocities determined from accepted theory are very high, and water thickness very low, often not more than a few centimeters. This case resembles the cases of grass spillway erosion treated extensively by the Natural Resources Conservation Service, Oklahoma, USA.

The empirical, energy of impact based equation developed by the Oklahoma school for calculating headcut advance will be applied in this report. No distinction will be made in this report between crest or slope scarps and no consideration will be given to the quality of the material - grass, asphalt, bare earth - above and below the scarp.

Theoretical developements of the Oklahoma school with regard to free overfall analysis combined with a deterministic (rather than empirical) approach to headcut advance are described in Appendix C. These developments were considered not to be the most efficient model developements for use in this study but are promossing for further more accureate discriptions of the head cut erosion process.

The head cut deepening and migration models are described using De Groot's (Deltares) calculations on the erosion of the core of the Diefdijk (section 5.2). The parameter choice and correlations with other soil parameters are described in section 5.3.

5.2 Synopsis of De Groot's report on the SSEA model

In the Deltares report "Erosion of the core of the Diefdijk during overtopping" (376270-0000, 2006, in Dutch), ir. M.B. de Groot subjects the Diefdijk failure to hypothetical overflows, and determines its resistivity to erosion. The hydraulic loading is first calculated using assumptions with regard to wave height frequencies during a storm, and this results in a distribution of overflow discharges throughout a storm (of 48 h duration). The potential erosion is calculated using the Sites Spillway Erosion Analysis methodology, which was developed by the Natural Resources Conservation Service of the USA.

In the following paragraph, De Groot's work with regard to erosion calculation will be presented.

De Groot notes that no reliable prediction models are available (2006) in the Netherlands for erosion of a dyke core consisting of clay due to storm wave overtopping. The US model SSEA, Sites Spillway Erosion Analysis, described in (NRCS 1997) however appears useful. Reference is made to chapters 51 and 52 of the SSEA manual.

The SSEA was developed for prediction of the erosion of earthen spillways downstream of earthen dams. Most such spillways are partially grass-covered Three erosion phases are distinguished:

Phase 1 The failure of the vegetal cover protection (if any) and the development of concentrated flow
Phase 2 The downward and downstream erosion associated with the concentrated flow that leads to formation of a vertical or near-vertical headcut in the vicinity of initial failure
Phase 3 The upstream advance and deepening of the headcut resulting from flow over the vertical or near vertical face

Phase 1 is not relevant in the present case. Phase 2 is shown in the figure below, and phase 3 in the following figure.

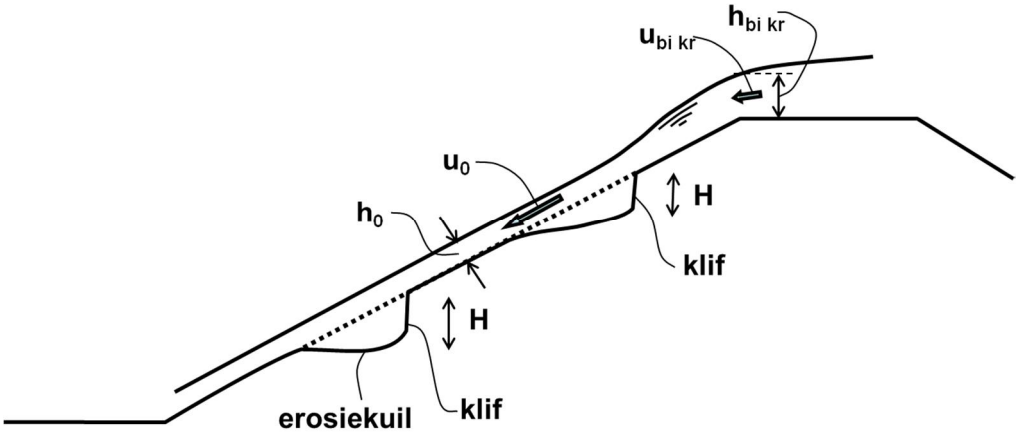

Figure 5.1 Phase 2 head-cut formation

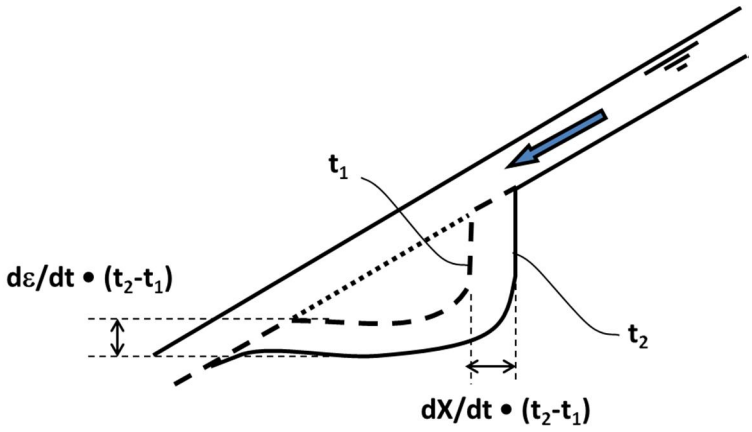

Figure 5.2 Phase 3 upstream advance of head-cut with velocity dX/dt and deepening dε/dt

The concentrated flow in Phase 1 is due to inflow from the sides. The flow accelerates and is super-critical. The rate of erosion in phase 2 is determined from the mass-wasting equation:

$$\frac{d\varepsilon}{dt} = k_d(\tau_e - \tau_c) \quad (5.1)$$

where k_d is the detachment rate coefficient ($ms^{-1}Pa^{-1}$), τ_e is the effective shear stress (Pa), and τ_c is the critical (threshold) shear stress (Pa). Note that k_d and τ_c are soil parameters, while τ_e is a hydraulic load. The rate coefficient k_d shares the time and length unit with the deepening rate $d\varepsilon/dt$. In the American literature in ft/hr, in this report also m/hr and m/s are used. The unit is systematically given in the report to avoid misunderstandings. The methodology prescribes the determination of τ_e, k_d and τ_c. The SITES manual states that the erosion depth at the end of Phase 1 is generally 0.5 foot (0.15 m).

In Phase 2 the erosion depth increases due to particle detachment of the denuded soil, and the same basic equation as for Phase 1 is used (eq. 5.1). The water falling over the headcut erodes it. At the base of the headcut erosion is at least as strong as at the head, and the headcut remains steep and advances upstream. This occurs only after the headcut has reached a certain height. Phase 3 therefore starts sometime after the beginning of Phase 2. But the headcut continues to increase in height during Phase 3 as well. The headcut advance is calculated using equation 5.2.

$$\frac{dX}{dt} = C(A - A_0) \quad (5.2)$$

where, dX/dt is the head cut advance (m/s), C is the advance rate coefficient ($s^{-2/3}$), $A=(qH)^{1/3}$ ($ms^{-1/3}$) where q is the specific discharge (m^2s^{-1}) and H (m) is the head cut height and finally A_0 ($ms^{-1/3}$) is the thresh hold parameter. Self evident, the parameters must share the same units. In the American literature foot and hours, in this report meters and hours or seconds. In the report the units are given to avoid misunderstandings.

The method has been validated against several hundred tests on spillways, and De Groot states that the method agrees well with observations in the Netherlands. Rather than use the SSEA software, which is rather involved, the pertinent equations are gathered in a spread sheet to enable simple application of the model.

Soil characteristics
Based on various field and laboratory tests, De Groot arrives at the following soil parameters for the clay core of the Diefdijk.

Soil type is Clay with varying amounts of sand and silt mixed in. Most common is weakly sandy clay and medium silty clay. Dry density is taken as 17.2 kN/m^3. Undrained shear strength is taken as 40 kPa (unconfined compressive strength is 80 kPa).

Mass wasting soil parameters are k_d and τ_c:
According to equation [51-8]

$$k_d = \frac{5{,}66 \cdot \gamma_w}{\gamma} \cdot \exp\left[-0{,}121 \cdot c_{\%}^{0{,}406} \cdot \left(\frac{\gamma}{\gamma_w} \right)^{3{,}1} \right] \text{ giving the result in } \left[\frac{ft/hr}{lb/ft^2} \right] \quad (5.3)$$

and, taking 1 ft = 0.3048 m and 1 lb = 0.4536 kg,

$$k_d = \frac{0{,}036 \cdot \gamma_w}{\gamma} \cdot \exp\left[-0{,}121 \cdot c_{\%}^{0,406} \cdot \left(\frac{\gamma}{\gamma_w} \right)^{3,1} \right] \text{ giving the result in } \left[\frac{m/hr}{Pa} \right] \quad (5.4)$$

where $c_{\%}$ is the clay percentage fraction.

According to Shields (figure 51-1 in NRCS 1997; see Appendix A) τ_c = 0,0025 lb/ft^2 = 0.12 Pa.[1]

The soil parameter for the headcut advance is K_h, for which [52-1] gives:

$K_h = M_s \,.\, K_b \,.\, K_d \,.\, J_s$ (5.5)

with (see Appendix A for tables and elaboration on the parameters copied from NRCS 1997):

- using table 52-3 an 'unconfined compressive strength' = 80 kPa M_s = 0,05
- From p 52-8 (above left) K_b = 1
- From eq. [52-10] $K_d \cong \tan \phi'_r \cong \tan 22° = 0.40$; where ϕ'_r is the residual friction angle
- From p 52-13 (above left) J_s = 1

Therefore: K_h = 0,05.0,40 = 0,02 (-)
The parameter is used to calculate the head cut advance rate parameter C (equation 5.19).

Calculation of erosion and formation of headcuts (phase 2)
The discharge q is given and is the same at the head of the slope and everywhere along it. Then the product of initial flow velocity v_0 and initial water layer thickness h_0 remains constant:

$$u_0 \cdot h_0 = q \quad (5.6)$$

Along the slope v_0 en h_0 will be determined such that the friction along the slope equals the force resulting from the hydraulic gradient. Chezy then applies:

$$\tau = \rho g h i = \rho g \cdot \left(\frac{u_0}{C_A} \right)^2 \quad \text{or} \quad (5.7)$$

$$u_0 = C_A \cdot h_0^{1/2} \cdot i^{1/2} = \left(\frac{h_0^{1/6}}{n} \right) \cdot h_0^{1/2} \cdot i^{1/2} \quad (5.8)$$

in which n [s/m$^{1/3}$] is the Manning coefficient which signifies roughness of the slope and i is the slope inclination (m/m).

It then follows that:

$$u_0 = q^{2/5} \cdot i^{3/10} / n^{3/5} \quad (5.9)$$

[1] *In Appendix B τ_c (Pa) is calculated to be considerably higher, in the order of 10-30 Pa, based work by Mirtskhoulava described in Hoffmans and Verheij 1997*

$$h_0 = q^{3/5} \cdot n^{3/5} / i^{3/10} \tag{5.10}$$

For denuded clay, SSEA gives (halfway between equations [51-16] en [51-17]) n = 0.02 s/m$^{1/3}$. For h = 0.1 m we then find C_A = 34 m$^{1/2}$/s.

> *Note 1 that the flow velocity and water layer thickness are calculated by using equilibrium between bed sheer stress and gravitational pull. This is a different approach than in section 4 where the flow velocity and water layer thickness were derived from an empirical relation between overtopping wave volume and the flow parameters on the crest. Field tests have shown that for 1:3 slopes the generated flow parameters by overtopping waves do not change much and are therefore close to the equilibrium parameters. For steeper slopes the flow accelerates and for gentler slopes the flow decelerates. In general, for the intermediate and common 1:3 slopes the parameter are in the same order of magnitude.*

Erosion rate dε/dt is given by SSEA-equation [52-2]:

$$d\varepsilon / dt = k_d (\tau - \tau_c) \tag{5.11}$$

leading to local scour of depth H and water depth h_0 + H.

According to SSEA the bottom shear stress in the scour hole increases proportionally to the water depth:

$$\tau = \rho g h i = \rho g i (h_0 + H) \tag{5.12}$$

If the flow is uniform, this would mean that the discharge in the scour hole is increasing and that flow is being concentrated towards the hole. But increasing shear stress can also be due to acceleration of the water entering the hole. If velocity is supercritical (Dutch: schietend water) then

$$\frac{u^2}{2g} \le \frac{u_0^2}{2g} + H \quad \text{or } \tau \le \rho g i (h_0 + H \cdot \frac{g}{C_A^{\,2}}) \approx \rho g i (h_0 + H \cdot 0{,}1) \text{ if } C_A \cong 34 \text{ m}^{1/2}/\text{s}. \tag{5.13}$$

The SSEA shear stress in the hole therefore is probably estimated too high, certainly if H > h_0 which will be the case when a significant amount of erosion has occurred.

An upper limit to the shear stress can be derived as follows:

$$\frac{u^2}{2g} = \frac{u_0^2}{2g} + H \quad \text{and} \quad \tau = \rho g \cdot \left(\frac{u}{C_A} \right)^2 \quad \text{with} \quad C_A = \left(\frac{h_0^{1/6}}{n} \right) \tag{5.14}$$

A third alternative is to take shear stress in the hole equal to that on the slope:

$$\tau = \rho g h_0 i \tag{5.15}$$

De Groot applies these three approaches to the Diefdijk case. The first approach gives unrealistically high shear stresses: a factor 20 - 50 increase for a 1 m deep hole. Such a depth is reached after only 15 minutes for a (continuous) discharge of 50 liter/m/s.

For the second approach they are lower but still appear to be rather high: 2 - 4 times higher for the 1 m deep hole. He decides to adopt the third approach with constant shear stress on the entire slope.

Using this third approach, the Diefdijk case subjected to the peak discharge during a design storm $q_{1\%}$ = 348 l/m/s (exceeded by 1% waves) results in a depth of erosion of 1 m in 0.7 h. Taking $q_{mean,NN}$ = 9,5 l/m/s to occur continuously, this would be 1 m in 6 h. Differentiating the discharge according to the expected distribution and height of waves, the erosion would amount to 4.8 m for a 48 h storm.

Calculation of headcut advance (phase 3)
An empirical equation determines rate of advance of the headcut:

$$dX/dt = C(A - A_0) \quad (5.16)$$

$$A = (qH)^{1/3} \quad (5.17)$$

$$A_0 = \left[189 \cdot K_h^{1/2} \cdot \exp\left(\frac{-3{,}23}{\ln(101 \cdot K_h)} \right) \right]^{1/3} \quad (5.18)$$

$$C = 3.04 - 0.79.\ln(K_h) \quad (5.19)$$

with A en A_0 in ft/s$^{1/3}$, and dX/dt in ft/hr. Note that the C also holds the transition between the unit hours (for dX/dt) and seconds (for A and A_0).

The advance is calculated for the same three cases as the second phase erosion. At peak discharge, advance rate is 3 m/h when the headcut is H = 1 m. It increases to 5 m/h when H = 3 m. The average discharge results in 0.1 m/h for a headcut of H = 1 m and increases to 0.7 m/h when H = 3 m. For the expected distribution of discharges during the 48 h storm, an advance of 14 m is calculated.

De Groot finally discusses his results. The 4.8 m depth of erosion in Phase 2 implies failure of the dyke even before the advance in Phase 3. Even if this erosion was concentrated at the lower part of the slope, the 14 m headcut advance would be enough for even a relatively wide crest of 6 m to vanish. Should the storm duration be not 48 h but 20 h, the figures would be 2 m of Phase 2 erosion and 2 to 3 m of headcut advance. A 6 m wide crest would barely survive this storm.

De Groot finds that by and large, the Sites model appears qualitatively correct and at high velocities at least appears to concur with flume tests carried out in the Netherlands. At lower velocities, using Shields probably results in too low values of the critical shear stress for erosion-resistant clays, and consequently overestimates of erosion.

De Groot is concerned about the calculation of shear stress and has the impression Sites is overly conservative, but is uncertain about the validity of his alternatives.

The Phase 2 analysis described by the De Groot will not be applied further in this report. It is considered that the scarp provides a pre-formed headcut which is ready to advance when subjected to overflow. Deepening of the headcut during the advance is therefore also not considered, but can be taken into account by choosing a conservative estimate of headcut height.

5.3 The Oklahoma research on rate of headcut advance

The Phase 3 headcut advance equation treated by De Groot, is also used in simpler form without the threshold value A_0 as

$$dX/dt = C\,(qH)^{1/3} \qquad (5.20)$$

Hanson and Cook (2004) describe flume tests and embankment overflow tests performed on 5 different soils in which the rate of headcut migration was determined. The soils are denoted by E, F (flume tests) and soil1, soil2 and soil3 (embankment overflow tests). They are either CL (low plasticity clay) and SM (silty sand) materials. According to the Dutch erodibility classification, which defines erodibility by zones in Casagrande's plasticity chart, see Figure 5.3, they fall in the 'highly erodible' category. We concentrate here on material E for which a total of 37 flume headcut migration tests were performed.

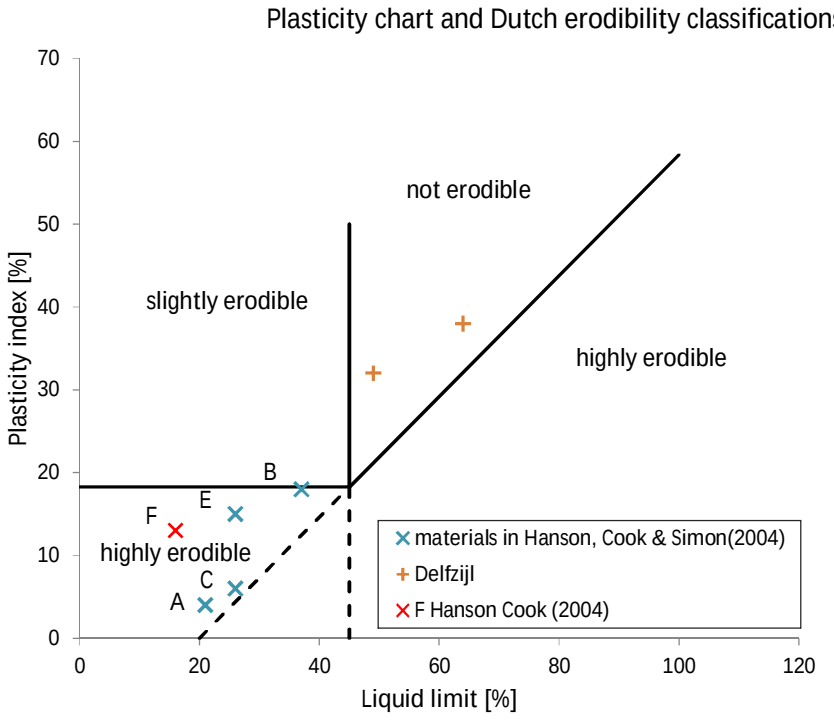

Figure 5.3 Dutch erodibilty classification, which defines erodibility by zones in Casagrande's plasticity chart

Pre-formed headcuts, H = 1.0 - 1.3 m were tested in flumes with discharges of q = 0.84 - 1.36 m^2/s (840 to 1360 liter/m/s). The figures below (Figure 5.4, Figure 5.5 and Figure 5.6) show the results in terms of dX/dt and parameter C, while the compaction characteristics of the materials are also shown.

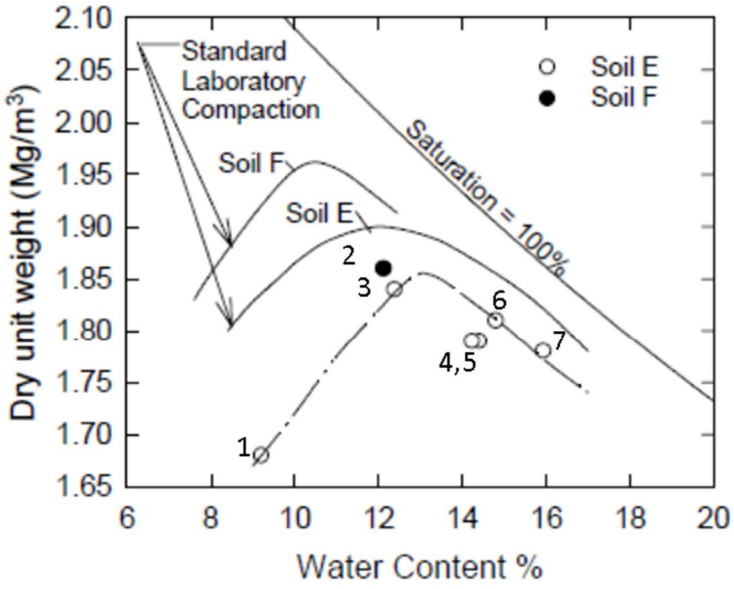

Figure 5. Compaction results for Soil E and Soil F in the laboratory and in the flume.

Figure 5.4 Water content (%) vs dry unit weight for soils E and F; Figure 5 taken from Hanson and Cook (2004)

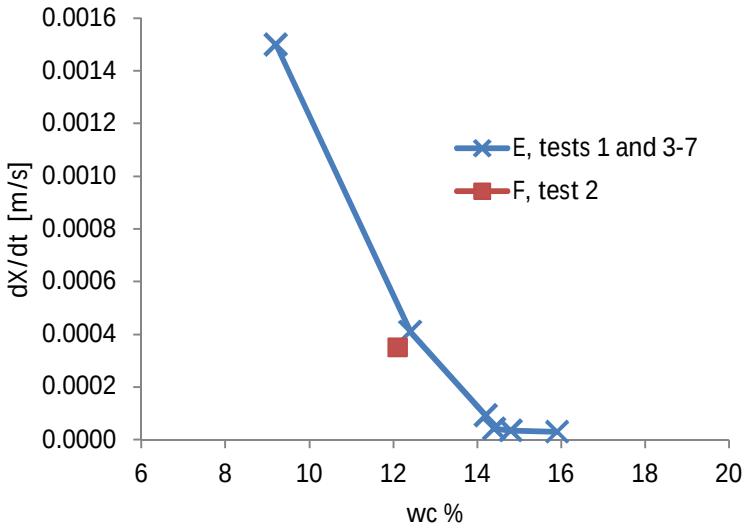

Figure 5.5 Water content wc (%) vs measured headcut migration dX/dt (m/s) for soils E and F

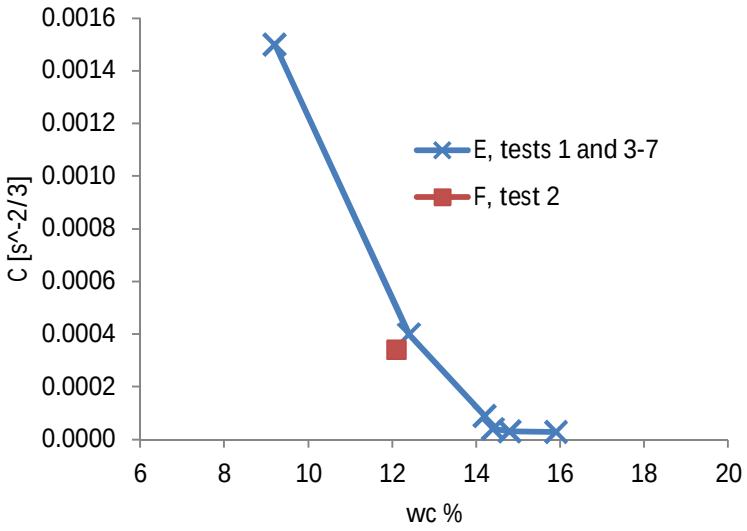

Figure 5.6 Water content wc (%) vs C ($s^{-2/3}$) back calculated from tests performed on soils E and F

Note that migration rate decreases with increasing (post-compaction) water content. The authors relate the two as

$$C = 3000(wc\%)^{-6.5}\ [s^{-2/3}] \qquad (5.21)$$

However, this correlation will be shown to break down for higher water content materials such as plastic clays, in which much too conservative (low) values of C are predicted. De Groot's C value for Diefdijk clay was 6.13 $s^{1/3}$/h or 0.0017 $s^{-2/3}$, which is higher than any value found by Hanson and Cook. De Groot followed the Sites procedure to determine C from a number of factors such as undrained shear strength, residual friction angle, particle size and soil structure, but Hanson, Robinson and Cook (2001) warn that "at present, there is no way of determining the material-dependent parameters without knowing the headcut migration rate". Correlations to determine C should therefore be treated with care.

In other work by the Oklahoma school, Hanson, Cook and Simon (1999), an important feature of erosion resistance is revealed. There, the k_d and τ_c parameters of the simple mass-wasting equation are given as found from laboratory jet erosion tests (Figure 5.7).

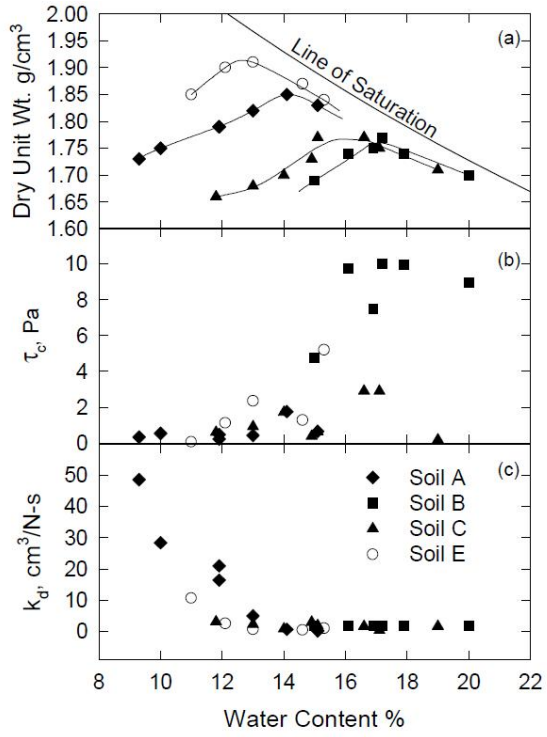

Figure 6. Effects of compaction water content on τ_c and k_d for soil A, B, C, and E.

Figure 5.7 Dry unit weight (g/cm^3), τ_c (Pa) and k_d(cm^3/N-s) vs water content (%) for soils A, B, C and E, Figure 6 taken from Hanson, Cook and Simon (1999)

The materials A, B, C and E are also shown in the plasticity chart above (Figure 5.3), where they all fall in the highly erodible category. But note that the above figure gives highly varying values for k_d and τ_c, depending not only on material plasticity, but also on water content relative to the proctor optimum. Wet of optimum, erosion resistance is much higher with low k_d and high τ_c values.

The Dutch standards with respect to clay to be used in dykes specifies that the consistency index I_c should be higher than 75%. It turns out that the bare clay of the Delfzijl overtopping tests (section 6) has I_c = 0.75, and flume tests on material E were also performed at I_c = 0.73 - 0.81.
With I_c > 0.75, water content is within 25% of I_p on the wet side of the plastic limit. As a rule of thumb, the proctor optimum occurs at 2 - 3 % water content below the plastic limit. In other words, Dutch clays are likely to be located well wet of optimum, in the zone of high erosion resistance according to the results in figure 6 of Hanson, Cook and Simons (1999).

Now taking a second look at the graph above of the flume test results from Hanson and Cook (2004) we see a similar trend - higher erosion resistance for material compacted wet of optimum. The effect is quite spectacular.

(Note also from the comparison of laboratory and field proctor curves on material E, that the field curve has lower density and slightly higher optimum water content than according to the laboratory curve.)

Knowing therefore that the Delfzijl clay lies well past optimum, and is much more plastic than the soils E and F tested in flumes by Hanson and Cook (2004), while its C value lies squarely within the range of the E and F results, the effects of the poor quality of the bare Delfzijl clay are apparent.

It is also concluded that the Diefdijk C parameter of De Groot is probably much too high.

Reliable data on the C parameter for plastic clays is lacking, let alone that the influence of I_c on C for such clays is known. However, for simple conservative estimations of erosion resistance of plastic clays, it would seem in order to take the value of C found by Hanson and Cook (2004) for the flume tests on the CL E material at high water content, which is:

$C = 3x10^{-5}\ s^{-2/3}$.

This value should be used without threshold value A_0.

For low plasticity clay, the field results for the E material at optimum water content could be used:

$C = 3x10^{-3}\ s^{-2/3}$.

6 Validation head cut advance for dikes with developed soil structure, Delfzijl and Bergambacht

The NRCS 1997 National Engineering Handbook part 628 Dams, is well suited for its particular purpose, however it might not be entirely applicable for describing breaching in typical Dutch dikes (Knoeff et al. 2002). The models and suggested parameters by the NRCS Handbook are therefor compared to two Dutch field tests.

First point of concern is the typical soil structure present in Dutch dikes (TAW 1996), which might not be incorporated in the suggested parameters by the NRCS. Soil structure develops as a result of the environment, changing moisture content due to draught and rain, frost, flora and fauna activities and (chemical) bonding between aggregates and grains. It takes time to develop and develops different for different soils and climates. The tested spillways, on which the NRCS models and parameter suggestions are based, are constructed and then tested, without sufficient time for soil structure to develop. Also the conditions, soils and climate, can be different from Dutch circumstances.

A second point of concern is the hydraulic load, which is more or less stationary in the spillway test conditions; however, for this study wave overtopping has to be taken into account. Wave overtopping gives a highly variable hydraulic load.

Within the framework of this study there are two cases available for validation of the models and parameters for the two points of concern: a wave overtopping test at a sea dike near Delfzijl (paragraph 6.1) and an overflow test on a river dike near Bergambacht (paragraph 6.2). Both dikes have sufficient 'age' to have developed soil structure. Reflection on the results will be given in section 6.3.

6.1 Wave overtopping erosion tests on Delfzijl sea dyke

6.1.1 Test set up and observations

The erosion by wave overtopping tests on the sea dyke at Delfzijl are described in Comcoast report Haskoning (2007). The test on a bare clay slope is considered here. The grass cover was removed by back hoes to a depth of 0.2 m. Flows were applied to the top of the slope as shown in Figure 6.1. Erosion holes developed halfway down the slope, and gradually a headcut formed which then migrated upslope. The rate of erosion and upslope migration can be determined from the figure (values read off from figure 12-5 of the Comcoast report). Note that the erosion depth does not increase after 14 hours. This is true for the initial location of the erosion hole, but as the headcut migrated upwards, headcut height increased to 0.98 m.

The average overtopping discharge was increased from 1-5-10 l/s/m each storm condition lasting for 6 hours. The average discharge was generated by a simulated sea state characterized by H_s=2 m and s_{0p}=4%. The distribution of overtopping wave volumes during the simulated sea state was divided in discreet volumes of 50-150-400-700-1000-1500-2000 l/m. The overtopping load in the Delfzijl case is given in Table 6.1.

1 l/s /m		5 l/s /m		10 l/s/ m	
l/m	Nr. in 6 hr.	l/m	Nr. in 6 hr.	l/m	Nr. in 6 hr.
50	54	50	225	50	384
150	54	150	123	150	252
400	9	400	81	400	147
700	6	700	30	700	57
1000	3	1000	12	1000	33
		1500	3	1500	9
		2000	3	2000	6

Table 6.1 Wave overtopping load Delfzijl in number of volumes during a 6 hour storm simulation for average discharges of 1-5-10 l/s/m (volumes randomly distributed during the overtopping simulation)

The average discharge, the measured head cut deepening and head cut advance are plotted against time in Figure 6.1.

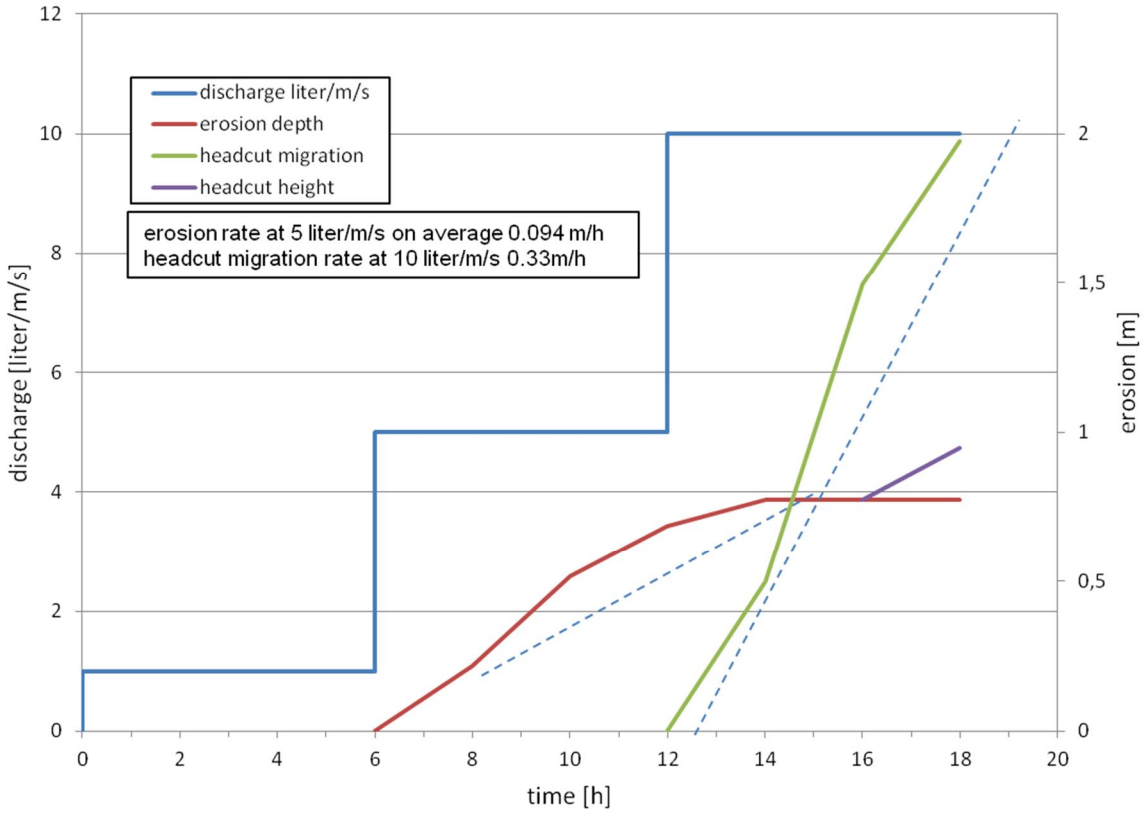

Figure 6.1 Average discharge (l /m/s) generated by a simulated sea state characterized by H_s=2 m and s_{0p} = 4%, erosion depth (m), headcut migration (m) and headcut height (m) against test time, for the Delfzijl overtopping test on bare clay. The hydraulic load was increased every 6 hours

During the 1 l/s/m average discharge load there was some surface erosion concentrated at obvious week spots caused by cranes which had stripped the grass sod from the slope to a depth of 0.2 m.

The authors of Comcoast (2007) point out that:

"The removal of the grass layer was realized by two cranes, a heavy crane working from the toe of the dyke and a smaller crane working from the crest. The reach of both cranes was limited and they did hardly overlap. Where the reach was maximum, they scraped the grass cover, while loosening the subsoil to some extent. This especially applied to the heavy crane at the toe of the dyke when it had its longest reach." (Figure 6.2)

Figure 6.2 Two cranes stripping the sod from the clay (ComCoast)

The erosion roughened the slope, however no distinctive scour holes were formed. During the 5 l/s/m test erosion starts to develop up to a depth of 0.7 m with a near vertical cliff. The erosion was almost continuously, and was not just caused by the largest wave volumes. Long after passage of the maximum flow of an overtopping wave the remaining flow converged strongly towards the scour hole continuing the erosion process. The scour hole did not yet migrate upstream. During the 10 l/s/m test the scour hole deepened to 1 m at the headcut and the formed headcut migrates upstream. Upstream of the distinctive scour holes, surface erosion continued to a depth of 5 to 10 cm.

A summary of observations and models to describe the observed erosion is given in Table 6.2.

q [l/s/m]	Duration [hr]	Local scour hole deepening [m/hr]	Headcut migration [m/hr]
1	6	not relevant	not relevant
5	6	0.097	0
10	6	0	0.33
Model:		$\frac{d\varepsilon}{dt} = k_d(\tau_e - \tau_c)$	dX/dt = C(A – A_0)

Table 6.2 Summary observed erosion at Delfzijl overtopping test and describing erosion models

The average rate of erosion in the hole is 0.097 m/h at an average discharge of 5 liter/m/s. The headcut migration got underway at 10 liter/m/s and occurred at a rate of 0.33 m/h.

6.1.2 Back calculation headcut deepening and migration

The scour hole deepening was back calculated using the mass wasting equation, governed by k_d (m/s/Pa) and τ_c (Pa). The hydraulic load during the i^{th} wave overtopping event $\tau_{e,i}$ (Pa) is calculated by using the triangular flow velocity profile at the dike crest as a function of overtopping wave volumes (see section 4). The maximum shear stress during the i^{th} wave overtopping event is calculated as follows:

$$\tau_{e,i,\max} = \rho g \frac{u_{i,\max}^2}{C_A^{\,2}} \quad and \quad C_A = \frac{\sqrt{g}}{\mathrm{K}} \ln\left(12 \frac{h_{i,\max}}{k_s}\right) \tag{6.1}$$

The Chezy coefficient requires the constant of Von Kármán (=0.4) and the Nikuradse roughness k_s (m) which is $3*D_{90}$ for hydraulically rough conditions. For the wave overtopping conditions on bare clay a roughness of 0.02 m was used, resulting in a range of C from 23-37 $m^{0.5}/s$, depending on the wave overtopping volume. The scour hole deepening per wave overtopping volume was calculated by integrating over the time where $\tau_{e,i}$ (t) > τ_c or (t_i-T), where ti (s) is the wave overtopping event duration and T is the time where $\tau_{e,i}$ (t) drops below the threshold τ_c (Figure 6.3).

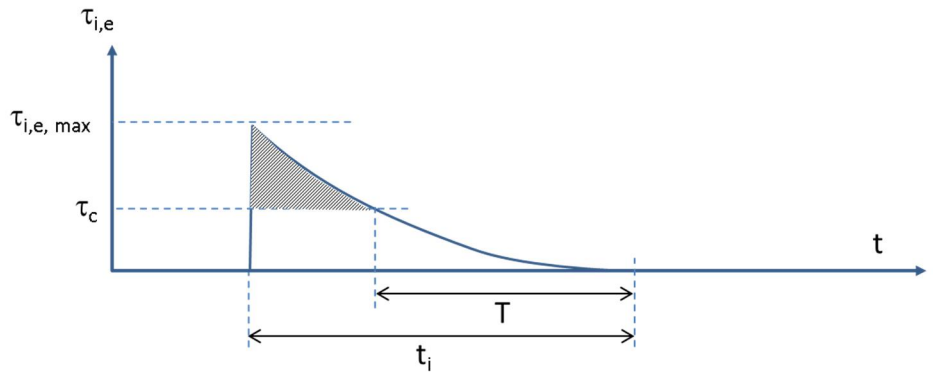

Figure 6.3 Integration where $\tau_{i,e}$ exceeds τ_c

$$\Delta\varepsilon_i = k_d \rho g \frac{u_{i,\max}^2}{3C_A{}^2 t_i^2}\left(t_i^3 - T^3\right) - k_d \tau_c \left(t_i - T\right) \quad where \quad T = \sqrt{\frac{\tau_c}{\rho g}} \cdot \frac{C_A t_i}{u_{i,\max}} \tag{6.2}$$

Each volume generating a load above the threshold strength adds to the deepening of the scour hole.

Estimates of τ_c (Pa), based on the plasticity index, void ratio and material description (clay or loamy clay), are given in Appendix B (taken from the Scour Manual). The clay at the Delfzijl test location has a liquidity index in the 0-0.25 range (low plasticity) and has a void ratio of about 0.75 (-) giving an estimated τ_c of 40-50 Pa.

Surface scour during the 1 l/s/m storm condition was very small. Surface scour remained within 0.2 m at the higher parts of the slope, even for the combined 1, 5 and 10 l/s/m load during a total of 18 hours. This would indicate that in the particle detachment or mass-wasting equation τ_c (Pa) can be relatively high, possibly due to the presence of roots deeper than the removed grass sod as noted in the ComCoast report.

As soon as a significant scour hole formed at the start of the simulated 5 l/s/m storm condition, the load increased locally and possibly the strength decreased due to absence of roots at larger depths beneath the slope surface. The deepening rate was 0.097 m/hr and occurred gradually, indicating that the treshhold parameter τ_c describing the deepening of the scour hole relatively low compared to the load by different sized overtopping wave volumes, and that it is much lower than τ_c describing the surface erosion process at 1 l/s/m and at the higher parts of the slope also for 5 and 10 l/s/m.

Given a threshold parameter τ_c = 40 Pa based on the Scour Manual (Appendix B), the deepening parameter k_d was fitted such that the calculated deepening met the observation. In order to resemble the observation it is necessary to have a higher k_d value for the soil between the slope surface and a depth of about 0.75 m, which would be about the depth of the main soil structure formation. The fitted deepening has a k_d = 3.5x10^{-5} m/s/Pa up to a depth of 0.75 m and then a decrease by a factor 10 to k_d = 3.5x10^{-6} m/s/Pa (Figure 6.4).

The NRCS hand book (Appendix A) suggests a τ_c near zero, and a k_d of 2x10^{-7} - 3.5x10^{-7} m/s/Pa, based on a clay content of 25-40% and a weight of 18 kN/m^3. With these parameters the deepening (a few centimetres) is underestimated considerably.

The headcut migration is modelled by dX/dt = C(A – A_0), where A = $(qH)^{1/3}$ and A_0 is a threshold value. The migration by a single overtopping wave i is calculated by:

$$X_i = C(H\, q_{i,\max})^{1/3} \int_0^{t_i} (1 - t/t_i)^{2/3}\, dt - C\, A_0\, t_i = \frac{3}{5} C\, A_{i,\max}\, t_i - C\, A_0\, t_i \tag{6.3}$$

Then by summation the total headcut advance during the storm is $X = \sum_i X_i$. For the head cut height in this calculation the observed values were used (Erosion depth and head cut height in Figure 6.4).

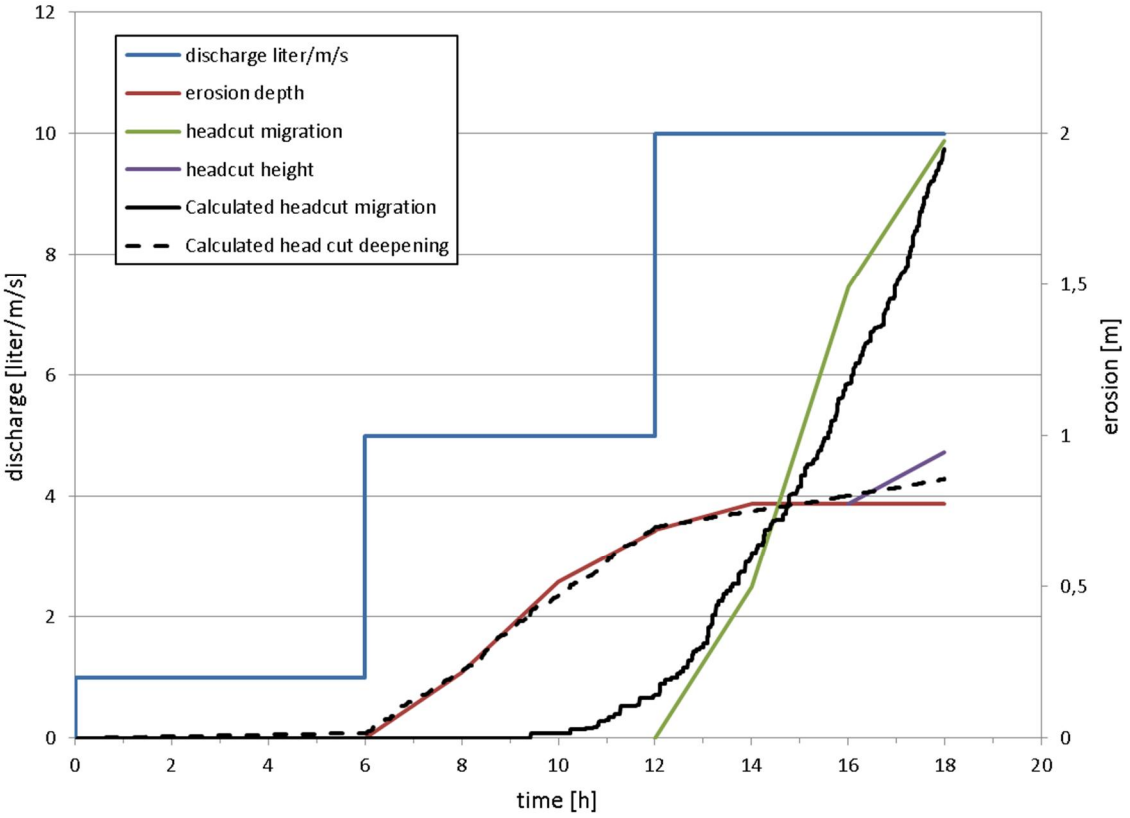

Figure 6.4 Observed and calculated (fitted) headcut deepening and migration at a wave overtopping test on bare clay at Delfzijl

Parameters A_0 and C were fitted such to fit the observed head cut advance. It was however impossible to fit the parameters exactly in a way that during the 5 l/s/m test the headcut migration is 0.0 m and during the 10 l/s/m test 2.0 m, as was observed. In order to have no headcut migration at all during the 5 l/s/m test the threshold value A_0 and should be equal to or larger than A for the largest load during the test, which were three volumes of 2000 l/m (Table 6.1). However, this 2000 l/m maximum load was also the maximum load during the 10 l/s/m test, although there were more of these maximum volumes in the 6 hour storm. If A_0 was larger than representing the 2000 l/m, than the headcut migration would also be 0 in the 10 l/s/m test. The measured erosion at this test shows however, that the threshold value is quite high relative to the load applied in Delfzijl.

With parameter A_0 = 0.37 ($ms^{-1/3}$) and parameter C=3x10^{-2} ($s^{-2/3}$) the predicted headcut migration during the 5 l/s/m test is 0.1 m and during the 10 l/s/m test 2.0 m which corresponds roughly with the test results (Figure 6.4). If A_0 is assumed 0, as suggested in section 5.3, C should be 1.5x10^{-2} in order to back calculate the final headcut migration.

The NRCS handbook (Appendix A) suggests an A_0 of 0 to 0.5, depending on the undrained shear strength and residual friction angle. For Delfzijl these parameters were not determined, however it probably is quite firm based on the high plasticity index, weight, lutum content and the feel of the material by handling it in the field. With an estimated residual friction angle $\phi_r' = 20^o$, and an undrained shear strength of 40 kPa (unconfined compressive strength 80 kPa; soft to firm in Appendix A) k_h=0.02 and A_0 = 0.2 $ms^{-1/3}$. Based on the same k_h=0.02, the

advance parameter C = 1.7×10^{-3} $s^{-2/3}$, according to Appendix B. With these parameters the head cut migration would start as soon as deepening occurred during the 5 l/s/m test and would be 0.6m at the end of the 10 l/s/m test, underestimating the head cut advance.

6.2 Overflow test Bergambacht

6.2.1 Test desciption

In a follow up of the macro-instability test at Bergambacht an overflow test was performed to investigate breaching after a slip failure (Koelewijn et al. 2002). The test set up is shown in the following photo's.

Figure 6.5 Experimental set up: 50 m sheet pile basin (right hand side) was filled to overflow the deformed crest after a slip failure (left hand side)

Figure 6.6 Detail of the scarp to be overflowed. Some remains of asphalt and or pavement elements founded on cemented sand and clay

The lowering of the crest due to the slip failure was estimated to be 1.4 m. The local scarp height where the overflow test took place was ca. 1 m judging Figure 6.8. The local scarp height was not reported in detail.

Figure 6.7 Overflow seen from the landward slope

Figure 6.8 Overflow over the landward slope, where no significant erosion (more than 0.2 m deep) occurred during the entire test

Figure 6.9 The head cut migrates outward, lowering the crest and concentrating the overflow, the scarp deepens into the pavement foundation (sand, caustic lime treated sand, gravel and clay) and undermines the asphalt on the deformed crest

In Figure 6.9 the water can be seen emerging from underneath the asphalt. The foundation material is eroded from underneath.

Figure 6.10 Close up of the head cut. The man in the yellow coat stands approximately at the original scarp location

Figure 6.11 Situation at the end of the test

6.2.2 Hydraulic load

The filling capacity of the basin was:

12:00	approximately 300 m^3/hr, start breaching, 100 m^3/hr through breach
12:00 - 12:45	45 minutes approximately 300 m^3/hr, lowering crest at breach
13:00 - 14:15	1:15 (hour:minutes) 1700 m^3/hr
14:30 - 16:00	1:30 (hour:minutes) 2500 m^3/hr

At first (12:00-12:15) the water overflowed a 10-12 m wide section, however, within 15 minutes the crest locally eroded, lowered, and the flow concentrated forming a breach. This happened within the first half hour of the test. From this time on, the complete discharge (minus leakage) flowed through the breach.

The concentrated flow in the breach spread over the remains of the former crest and asphalt road and gave an estimated load on the inner slope of 1:15 (hour:minutes) 40 l/s/m and 1:30 (hour:minutes) 57 l/s/m.

6.2.3 Head cut migration process

After half an hour into the test the initial scarp left after the slip failure, was divided in two cliffs, the *upper cliff* in sand protected by some grass, where the sand eroded in minutes, and the *lower cliff* in stiff clay covered by asphalt (locally) and a hard layer of sand treated with caustic lime.

The *upper cliff* migrated upstream as sand above the hard layer was eroded. As the grass sod sank in after the eroding sand, the crest lowered increasing the discharge through the breach. After two hours the head cut migration of the upper cliff came to a near stop, as all the sand was eroded and clay, with soil structure, and grass sod remained.

At the lower cliff the sand and loose soil in the fissure left by the slip failure eroded quickly. Also the sand underneath the asphalt was eroded, undermining the asphalt road (Figure 6.9) after 3:30 (hour:minutes) into the test. The erosion hole in the end reached about 0.1 - 0.2 m beneath the sand layer. The deepening of the erosion hole in the clay was limited. At the end of the test the head cut had advanced over about 1.3 m (ca. 0.45 m per hour) over a height of 1.5 m.

The schematised geometry at the start and finish of the test are given in Figure 6.12 and Figure 6.13.

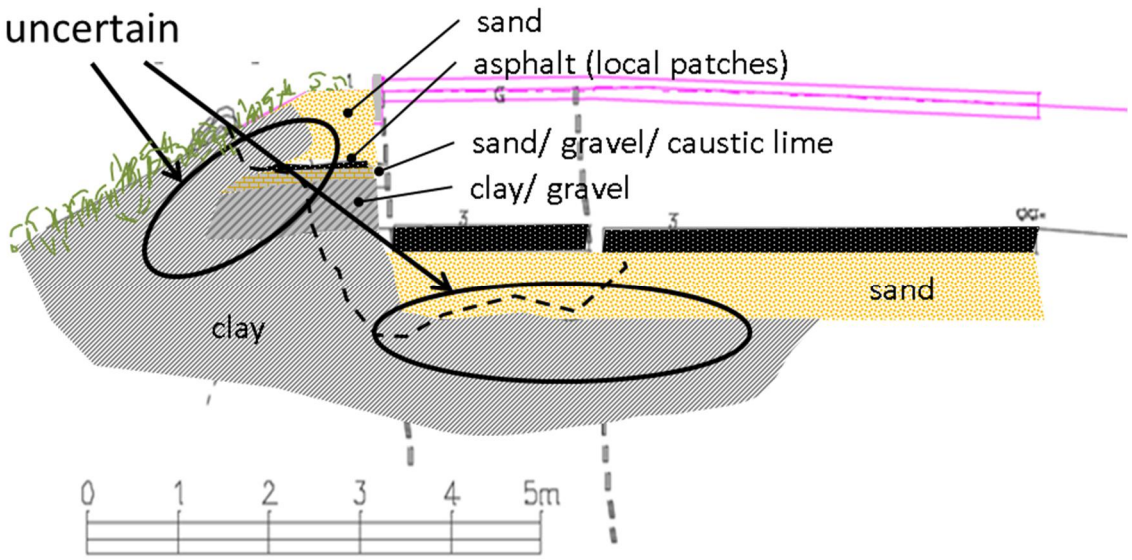

Figure 6.12 Schematized representation of the geometry before overflow test

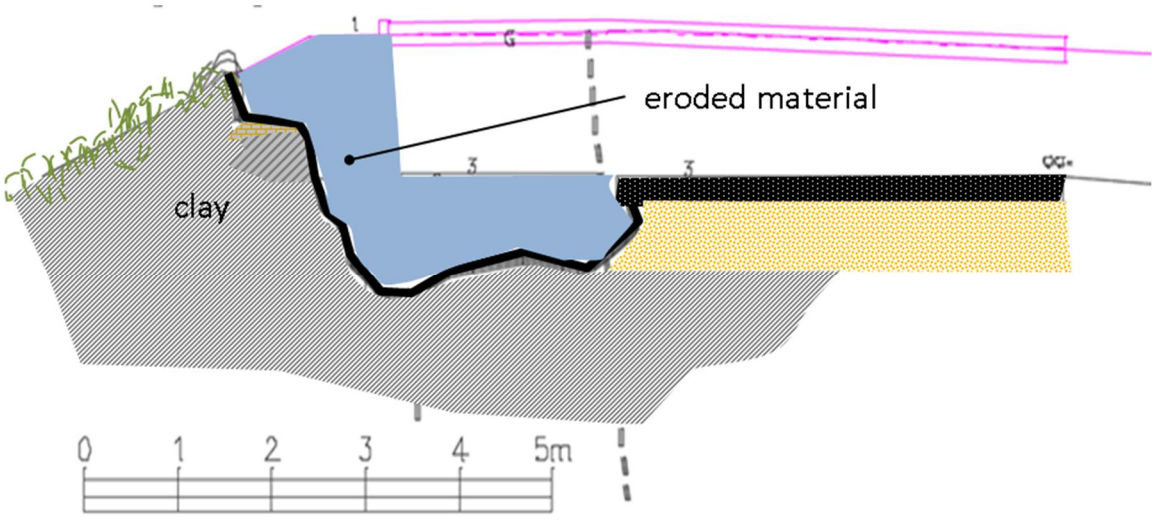

Figure 6.13 Schematized representation of the geometry after ending the test.

6.2.4 Back calculation of head cut advance Bergambacht

On average, the scarp migrated ca. 1.7 m upstream and developed in depth from 1 m to 1.5 m during the entire test. The back calculation of the head cut advance is governed by the advance parameter C ($s^{-2/3}$) and threshold parameter A_0 ($ms^{-1/3}$).

The combination of A_0 =0.2 $ms^{-1/3}$ (k_h = 0.02, see Appendix A) and C = $3x10^{-4}$ $s^{-2/3}$ gives a head cut migration close to the observation. If the threshold value is 0 than C = $2x10^{-4}$ $s^{-2/3}$ gives the observed head cut advance.

For the clay at Bergambacht (some soil data is given in Table 6.3), the NRCS Handbook suggests C = $1.5x10^{-3}$ - $2x10^{-3}$ $s^{-2/3}$ and threshold parameter A_0=0-0.5 $ms^{-1/3}$. The actual input parameters to determine the parameters A_0 and C are the undrained shear strength and residual angle of internal friction (see Appendix A). The parameters A_0 and C predict a

headcut migration of 4,5 to 17 m, which is much larger than observed and applying the NRCS parameters would have resulted in a breaching analyses on the safe side.

sample	depth	γ_{nat}	γ_{droog}	Wn	W_l	W_p	P_I	>2.8 mm	>63µ (sand content)	2-63µ	<16µ	lutum
no.	m	t/m^3	t/m^3	% (M/M)	% (M/M)	% (M/M)	% (M/M)	% (M/M)	% (M/M)	% (M/M)	% (M/M)	% (M/M)
125	1.00	2.13	1.78	19.8	39.6	20.3	19.2	16.9	33.8	48.1	45.9	18.2
126	1.40	2.02	1.63	23.8	39.6	19.1	20.5	0.0	27.1	50.0	48.1	22.9
127	0.15	1.92	1.45	32.7	53.3	23.1	30.1	0.0	27.0	42.9	56.3	30.1

Table 6.3 Soil characteristics Bergambacht, sample 125 from clay/gravel layer and sample 126 from the clay core (see Figure 6.12). Sample 127 is from the landward slope

6.3 Summary of back calculated and NRCS Handbook parameters and reflection on the results

The parameter summary is given in Table 6.4.

Test	Parameter	Obser-vation	NRCS Best guess	NRCS Range for clay
Delfzijl deepening	τ_c (Pa) k_d (m/s/Pa)	40 3.5×10^{-5}	0.12 3×10^{-7}	negligible 3×10^{-6} - 1×10^{-7}
Delfzijl deepening if τ_c=0	τ_c (Pa) k_d (m/s/Pa)	0 1.5×10^{-5}		
Delfzijl migration	A_0 ($ms^{-1/3}$) C ($s^{-2/3}$)	0.37 3×10^{-2}	0.2 1.7×10^{-3}	0-0.5 1.5×10^{-3} - 2×10^{-3}
Delfzijl migration if A_0=0	A_0 ($ms^{-1/3}$) C ($s^{-2/3}$)	0 1.5×10^{-2}		
Bergambacht migration	A_0 ($ms^{-1/3}$) C ($s^{-2/3}$)	0.2 3×10^{-4}	0.3 1.6×10^{-3}	0-0.5 1.5×10^{-3} - 2×10^{-3}
Bergambacht migration if A_0=0	A_0 ($ms^{-1/3}$) C ($s^{-2/3}$)	0 2×10^{-4}		

Table 6.4 Summary of back calculated parameters and NRCS Handbook parameters (Appendix B)

6.3.1 Deepening

The deepening rate at the Delftzijl wave overtopping test was an order of magnitude quicker in the upper layer (0-0.75 m) than would be expected based on the range of NRCS parameters. An explanation can be found in the soil structure at Delfzijl, enhanced by the back hoe scraping action to remove the grass sod exactly at the spot where most of the erosion took place (paragraph 6.2.1). At greater depth the deepening rate slowed to a rate within the NRCS range (1×10^{-6} m/s/Pa).

For safety it is recommended to incorporate a margin for disturbed soil with soil structure, with a high deepening rate k_d. The Delfzijl case can be used as an upper limit (0.8 m with k_d=1x10^{-5} m/s/Pa). The deepening rate affects the head cut migration process because it increases the scarp height H.

An easy and practical way to account for possible high deepening rates in the top layer with (disturbed) soil structure is to increase the scarp height with which the head cut migration is calculated. For the six storm conditions (section 4) the deepening within a storm is given in Table 6.5 for the upper limit of k_d in clay with soil structure (Delfzijl value), the upper limit of the NRCS range (3x10^{-6} m/s/Pa) and the approximated deepening if the Delfzijl material is limited to 0.8 m.

Headcut deepening (m)	q=1 l/s/m			q=10 l/s/m		
	Hs=2	Hs=1	Hs=0,5	Hs=2	Hs=1	Hs=0,5
τ_c=0 Pa; k_d=1x10^{-5} m/s/Pa	0.12	0.24	0.49	1.05	1.66	2.46
τ_c=0 Pa; k_d=3x10^{-6} m/s/Pa	0.04	0.07	0.15	0.31	0.50	0.74
Disturbed soil to depth 0.8 m	0.12	0.24	0.49	0.87	1.06	1.30

Table 6.5 Headcut deepening (m) within a 6 hour storm condition characterized by Hs=0.5; 1; 2 m and q=1 and 10 l/s/m for disturbed soil (Delfzijl kd=1x10-5 m/s/Pa) erodible soil NRCS (k_d=3x10^{-6} m/s/Pa and disturbed soil to 0.8 m with erodible NRCS soil underneath

The maximum deepening under the assumption of 0.8 m of disturbed soil and underneath the high end of erodible soil according to the NRCS Handbook, will be at the end of the storm. It is therefore recommended to add half of the calculated deepening to the scarp height needed to calculate the headcut advance, roughly 0.25 m for the 1 l/s/m average overtopping discharge and 0.7 m for the 10 l/s/m case.

Note that these are rough estimates, keeping safety in mind. The actual process of deepening is non-linear and complex. Much depends on the material properties at the bottom of the overtopped scarp. If this is for instance asphalt or grass the deepening rate will be much slower and might even be zero for the storm durations and conditions at hand.

The calculated deepening increases with decreasing wave height for a given average overtopping discharge. This means the high frequency of small overtopping discharges is more erosive than the less frequent high discharge events, given the same average discharge q. This holds especially for the no threshold case τ_c=0 Pa. If a higher threshold is taken, such as 40 Pa proposed in Appendix B, than the deepening decreases for decreasing wave height. In reality the deepening will probably decrease again when the overtopping tends to overflow at low average discharges. The momentum of waves giving extra flow velocity become unimportant and a more or less stationary spillway flow will develop. At a low overtopping rate of 1 or 10 l/s/m this means a very thin water layer at relatively low speed. A 1 l/s/m discharge simulated at a test on a grass slope did hardly show, because most of the water layer remained in between the grass plants.

6.3.2 Headcut migration

The head-cut migration rate C at Delfzijl was also an order of magnitude higher than the NRCS range, which could mainly be explained by the presence of soil structure and partially by the damage done by the back hoes. If the threshold parameter A_0 is taken equal to 0, as suggested in section 5.3, the advance rate parameter has to be the same order of magnitude as the NRCS range. The assumption of $A_0 = 0$ is however in conflict with the observation where no migration took place in the 5 l/s/m test and migration started at the 10 l/s/m test.

Apart from the unfavorable soil conditions at Delfzijl, also the way the wave overtopping load is taken into account, as opposed to the stationary flow used in the NRCS Handbook, can be an explanation for the differences. It is possible the triangular shaped overtopping wave volumes (section 4), should be taken into account differently, probably more stretched. It was observed that even some time after a wave overtopping volume had passed, cliff instability still took place. The relatively small remainder of the water on the slope, after passing of the main water volume, converged to the erosion hole (3D effect) and instability still occurred after passing of the main volume. The clean-up of instability debris in the erosion hole still requires a significant overtopping volume, however, the headcut instability part of the headcut migration process requires time and only a small discharge. This observation suggests it might be better to characterize the wave overtopping load by a longer time (in combination with a smaller discharge to balance the total amount of overtopping). A study to verify the observation and quantify the effects is beyond the scope of this study. Within this study a safety margin is applied to account for uncertainties.

The Bergambacht parameters from observation are an order of magnitude lower than the values given by the NRCS Handbook. If the fast erosion of the sand in this test is not taken into account the values are even somewhat further apart.

In conclusion. the parameters suggested by the NRCS Handbook (Appendix A) would have led to an under estimation of the Delfzijl head cut advance and a significant over estimation of the Bergambacht head cut advance. For the Delfzijl case, because of the scraping action of the crane removing the grass sod, it is likely that the soil condition was unfavorable to 'normal' conditions after an initial slip failure. A head cut advance rate based on the Delfzijl case would be too conservative especially when not taking into account a threshold parameter A_0. For both Delfzijl and Bergambacht no significant erosion was observed at a discharge of 1 l/s/m.

Given parameter range from the NRCS Handbook and the test results at Delfzijl and Bergambacht the following parameters are recommended to calculate the head cut advance in case of a slip failure.

Plastic, erosion resistant clay (TAW 1996)	$C = 1.5 \times 10^{-3}$ [$s^{-2/3}$] and $A_0 = 0.1$ [$ms^{-1/3}$].
Low plasticity erodible clay (TAW 1996)	$C = 2 \times 10^{-3}$ [$s^{-2/3}$] and $A_0 = 0$.
Sand	No erosion resistance.

Note that the threshold value A_0=0.1 $ms^{-1/3}$ equals a threshold momentary discharge of 1 l/s/m if the scarp is 1 m and 0,3 l/s/m if the scarp is 3 m.

The headcut migration during a storm condition giving 6 hours of overtopping (see section 4), is calculated for three scarp heights: 1, 2 and 3 m where in the calculations 0.3 m and 0.7 m are added to account for deepening (section 6.3.1). The scarp height follows from stability calculations. The results are given in Table 6.6 to Table 6.9.

average discharge over 6h storm: 1 l/m/s								
			highest wave			head cut migration [m]		
						C [$s^{-2/3}$] resp. A_0 [$ms^{-1/3}$]		
H_s	N	T_p	V_i	q_i	t_i	$1.5x10^{-3}$ / 0.1 erosion resistant clay		
[m]	[-]	[s]	l/m	l/m/s	s	scarp 1 m	scarp 2 m	scarp 3 m
0.5	1570	2.83	165	147	3.4	0.3	0.45	0.57
1	494	4.00	419	320	3.9	0.22	0.3	0.36
2	133	5.66	1130	737	4.6	0.13	0.17	0.2

Table 6.6 Headcut migration for q=1 l/s/m and Hs=0.5. 1 and 2 m, erosion resistant clay

average discharge over 6h storm: 1 l/m/s								
			highest wave			head cut migration [m]		
						C [$s^{-2/3}$] resp. A_0 [$ms^{-1/3}$]		
H_s	N	T_p	V_i	q_i	t_i	$2x10^{-3}$ / 0 erodible clay		
[m]	[-]	[s]	l/m	l/m/s	s	scarp 1 m	scarp 2 m	scarp 3 m
0.5	1570	2.83	165	147	3.4	1.03	1.25	1.41
1	494	4.00	419	320	3.9	0.53	0.64	0.73
2	133	5.66	1130	737	4.6	0.25	0.3	0.34

Table 6.7 Headcut migration for q=1 l/s/m and Hs=0.5. 1 and 2 m, erodible clay

average discharge over 6h storm: 10 l/m/s								
			highest wave			head cut migration [m]		
						C [$s^{-2/3}$] resp. A_0 [$ms^{-1/3}$]		
H_s	N	T_p	V_i	q_i	t_i	$1.5x10^{-3}$ / 0.1 erosion resistant clay		
[m]	[-]	[s]	l/m	l/m/s	s	scarp 1 m	scarp 2 m	scarp 3 m
0.5	5564	2.83	577	419	4.1	2.68	3.44	4.03
1	2433	4.00	1153	749	4.6	1.94	2.42	2.8
2	916	5.66	2562	1465	5.2	1.25	1.53	1.75

Table 6.8 Headcut migration for q=10 l/s/m and Hs=0.5. 1 and 2 m, erosion resistant clay

average discharge over 6h storm: 10 l/m/s								
			highest wave			head cut migration [m]		
						C [$s^{-2/3}$] resp. A_0 [$ms^{-1/3}$]		
H_s	N	T_p	V_i	q_i	t_i	$2x10^{-3}$ / 0 erodible clay		
[m]	[-]	[s]	l/m	l/m/s	s	scarp 1 m	scarp 2 m	scarp 3 m
0.5	5564	2.83	577	419	4.1	6.1	7.1	7.9
1	2433	4.00	1153	749	4.6	3.9	4.6	5.1
2	916	5.66	2562	1465	5.2	2.3	2.6	2.9

Table 6.9 Headcut migration for q=10 l/s/m and Hs=0.5. 1 and 2 m, erodible clay

The headcut advance increases with decreasing wave height for a given average overtopping discharge, as was the case for the headcut deepening. Although the highest waves per storm loading case lead to the higher rates of erosion as H_s increases, the build-up of the storm and the distribution of wave heights and durations is such that higher H_s leads to less total erosion. This may be an unexpected, contra-intuitive result, but is explained by the low power of 1/3 to which the impact energy qH is subjected in the equation for rate of headcut advance and the relatively low threshold value A_0. A storm with relatively few but high energy waves such as when H_s is larger, therefore may produce less erosion than a storm with many low energy waves.

This is exemplified in the following charts for the case of low-plastic clay (Figure 6.14).

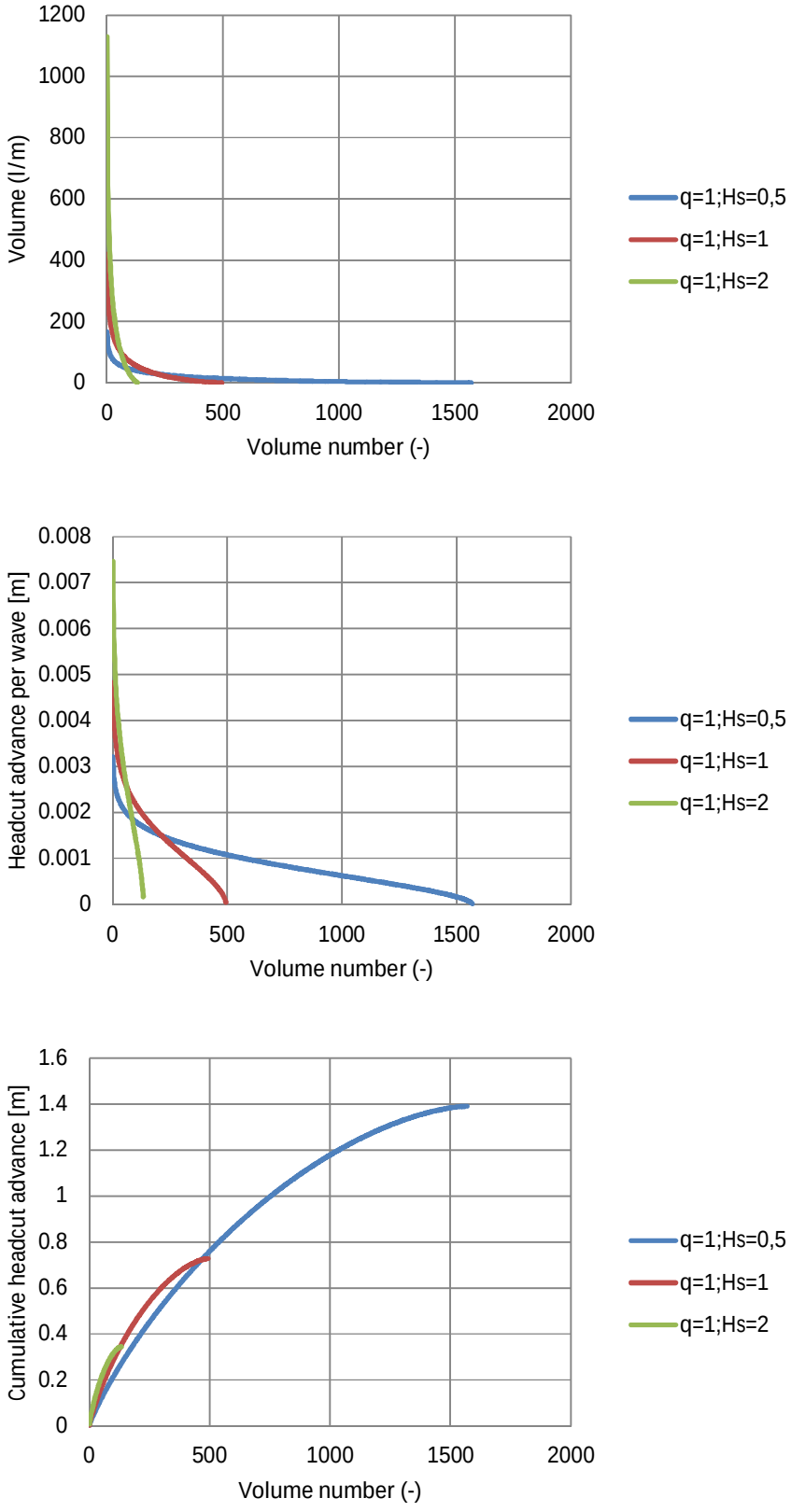

Figure 6.14 Overtopping wave volume (l/m), headcut advance per wave (m) and cumulative headcut advance during a 6 hour storm condition characterized by q=1 l/s/m and Hs=0.5;1 and 2 m

While the volume per overtopped wave is very high for H_s = 2 m, and the headcut advance is much stronger for the higher waves, the small amount of waves finally results in a smaller total advance. However, if a higher threshold value A_0 is used, such as the upper limit of the NRCS range for clay, than the headcut advance would be larger for the high wave storm condition.

The large discrepancy should perhaps not be wondered at. Viewing the extraordinarily large range of the C - parameter in the tests by Hanson and Cook (section 5.3), just by varying compaction water content of one and the same material, it is easily understood. While the recommended data set is provided with viable argumentation, if the Delfzijl and Bergambacht data is considered to reflect Dutch circumstances well it should evidently be preferred, above the Oklahoma data set.

The calculation for low-plastic highly erodible clay produces up to 7.9 m of headcut advance, which in most cases would be unacceptable. This concerns the H_s = 0.5 m case with an average discharge of 10 l/m/s. If the average discharge is 1 l/m/s, then a maximum headcut migration of 1.4 m is calculated, which in most cases would be acceptable.

7 Conclusions and recommendations

7.1 Conclusions

A slip failure does not lead to a dike failure and breaching, if a sufficient part of the dike crest remains intact. This is called residual strength after an initial slip failure. In Dutch practice, the guidelines in the technical report (Technisch Rapport Actuele Sterkte van Dijken) can be followed to determine if a potential slip plane endangers the water retaining function or not. The guideline takes into account the effect of secondary slip failures after the initial one, the secondary failures 'consuming' more dike material. However, the method excludes dikes which have an average overtopping discharge of more than 0.1 l/s/m.

Because many dikes are now designed based on a 1 l/s/m overtopping criterion, giving lower needed crest levels, and due to higher hydraulic loads and higher safety standards dikes tend to encounter more overtopping in safety assessment, there is a need to investigate whether the overtopping criterion of 0.1 when considering residual strength can be stretched.

This study shows indeed that if an extra safety margin in crest width is taken into account, the dike can still have residual strength after an initial slip failure if the average discharge is larger than 0.1 l/s/m.

If the dike is made of clay and the average overtopping discharge is not more than 1 l/s/m the scarp left by the initial slip failure can migrate outward by 1.5 m (calculated maximum of 1.41 m). If this extra margin in crest width is taken into account, on top of the margin taken for secondary slip failures, the residual strength of the dike can still be sufficient at 1 l/s/m overtopping.

For clay dikes and an overtopping discharge of 10 l/s/m the extra calculated margin increases to more than 7 m, which is not recommended for use at this stage of the study.

For sand dikes in combination with overtopping at a rate of more than 0.1 l/s/m, it is recommended not to take into account any residual strength based in this study. Sand proved to erode quickly, in the order of tens of minutes cubic meters of sand can potentially be lost. When considering the safety margin for erosion, it is recommended to discard sand and loose granular layers, for instance road foundations intersected by the scarp (think of them as being lost in a short time).

The conclusions have to be seen in light of several assumptions and simplifications, given in the report. Some of the main ones:

- The remaining soil body after the initial slip failure, the scarp height H (m) and place in 2D cross section is determined by a geotechnical stability calculation, which is not described in this report (see Technisch Rapport Macrostabiliteit Dijken). For the erosion calculation a scarp height up to 3 m was considered. The scarp can be in the crest, berm or slope. No distinction is made in this study.
- The wave overtopping is characterized by an average discharge q (l/s/m), a significant wave height H_s (m), a wave steepness of 4% (deep water and peak period). Two average discharges of 1 and 10 l/s/m were considered and 3 H_s' of 0.5, 1 and 2 m. (Note, the conclusion above is recommended for the 1 l/s/m condition, it is not recommended stretch the use of this conclusion by interpolation between the 1 and 10 l/s/m result without further study.)

- The overtopping condition was taken constant over a period of 6 hours, representing a storm peak of a few hours and accounting for the storm flanks. It is assumed to be equivalent, or even a bit on the safe side, to the actual hydraulic load if the storm and water level development in time were taken into account precisely. It is assumed this holds for all Dutch water systems, also the upper river area and the Eastern Schelde. Some safety is incorporated by the assumption that the slip failure occurs before or at the start of the wave overtopping event.
- The flow velocity, water layer thickness and their development in time (per overtopping volume) at the crest is taken for erosion calculations. Acceleration on steep slopes or deceleration on gentle slopes, crest or berms is neglected.
- The erosion analyses were done using the formulae for headcut deepening and migration given by the NRCS Hand book for dams (NRCS 1997). Also the parameters suggested by the Handbook were considered (Appendix A), together with parameters back calculated from two validation cases (Delfzijl and Bergambacht) when determining the parameters for concluding erosion calculations. It is likely that the erosion parameters used to calculate the headcut migration at 1 l/s/m are sufficiently safe for Dutch conditions, however when studying the subject it became obvious that the problem is complex and extrapolations beyond 1 l/s/m should be done with care and caution.
- Erosion due to a preferential flow through fissures parallel to the dike and bending towards the polder, the 3D slip plane fissures, was considered not to be normative, based on observations at Bergambacht. It was also considered plausible that a water flow with some momentum perpendicular to the dike does not concentrate easily in directions parallel to the dike (low momentum overflow could possibly be more susceptible to flow through these fissures).

7.2 Concluding text for Technisch Rapport Macrostabiliteit Dijken (Dutch)

The following text will be entered in the (CONCEPT) Technisch Rapport Macrostabiliteit Dijken:

In het kader van het WTI2017 onderzoek reststerkte na macro-instabiliteit (Residual dike strength after macro-instability [ref. 52]) is gekeken naar de mate van de te verwachten erosie na een afschuiving bij golfoverslag . Door een afschuiving ontstaat een bijna verticale klif die als gevolg van erosie door golfoverslag stroomopwaarts kan migreren over een bepaalde lengte. In de literatuur staat dit bekend als headcut erosie. De benodigde restkruinbreedte voor de situatie tijdens MHW of Toetspeil, kan in geval van golfoverslag met deze erosielengte worden vergroot.

Voor het berekenen van de erosie door golfoverslag na een binnenwaartse afschuiving moet rekening moeten worden gehouden met de erosiebestendigheid van de grond en de golfoverslagbelasting, bestaande uit het overslagdebiet, de golfhoogte en de tijdsduur. Uit het onderzoek volgt dat de modellen nog onvoldoende zijn gevalideerd voor de specifieke toepassing van headcut erosie door golfoverslag na een afschuiving, om de erosielengte precies te berekenen. Wel is het mogelijk gebleken om voor een kleiondergrond een veilige waarde te geven voor een overslagdebiet van 1 l/s/m. Voor overslagdebieten tot 1 l/s/m bedraagt de erosielengte in klei maximaal 1,5 m. Voor een overslagdebiet van 10 l/s/m is weliswaar een erosielengte bepaald maar gezien de onzekerheden in de studie wordt het niet aanbevolen daarmee te rekenen. Voor een zandondergrond wordt aanbevolen geen rekening te houden met reststerkte.

7.3 Recommendations

A first recommendation is to discuss the outcome of this study with RWS WVL, possibly someone from ENW and others to investigate whether the conclusions will hold in an ENW publication and what further investigations could be useful. This discussion was part of the work description.

Suggestions for further work, pending the outcome of the discussion:

- To find more cases of levees or dikes with developed soil structure which have (nearly) failed by overtopping and sliding and where the hydraulic load can be estimated (overtopping discharge and time). The two cases analysed in this study provided confidence in the chosen erosion parameters, more cases would strengthen this confidence so the results could be extended to higher loads (for instance 5 or 10 l/s/m).
- Find ways to investigate the erosion rate parameters and threshold parameters from the field. Correlations based on laboratory test results tend not to incorporate the effects of developed soil structure which is important for the erosion process. There are field water jet testing devices which could be useful in this, however, there will be work needed to determine the parameters from the field observations using the jet type devices.
- As illustrated by the case of Bergambacht dikes can be notoriously inhomogeneous. Former road foundations of granular material and sand can be present in the dike, and can erode quickly. For dike design it is a good to know that these materials have almost no residual strength when it comes to erosion. For safety assessment it is important to know whether these materials are present and where they are. It is recommended to develop a method to determine the presence of these materials in the dike profile.
- The models used in this study could be improved as shown in sections 5.4 and 5.5. Also erosion modelling now developed for residual strength in cases of a failed revetment in wave impact conditions could be checked for the applicability of erosion in case of overtopping. Research has been on-going since the NRCS Handbook appeared and could be used to describe the erosion process more accurately.

References

TAW 1994. Handreiking Constructief ontwerp (Dutch guideline in dike design). Onderzoek en berekening naar constructief ontwerp van dijkversterking

TAW 1996. Technisch Rapport Klei voor Dijken. Delft

TAW 2002. Technisch Rapport Golfoploop en Golfoverslag bij Dijken (Dutch guideline on wave overtopping and wave run up). Technische Adviescommissie voor de Waterkeringen. Delft mei 2002. Druk NIVO Delft

ENW 2009. Technisch Rapport Actuele Sterkte van Dijken (Dutch guideline in dike design and safety assessment). gedetailleerde en geavanceerde methoden voor de beoordeling van de macrostabiliteit binnenwaarts. Expertisenetwerk Waterkeringen. 27 maart 2009

GeoDelft 2002. Beoordeling binnenwaartse stabiliteit op basis van zoneringsmethode. Projectnummer CO-390110/34. mei 2002

Proefvak Bergambacht Evaluatierapport. Delft Cluster report 710301/334. june 2002. ir. J. Lindenberg 167p

Overloop- en bresgroeiproef. Proefvak Bergambacht. Delft Cluster report 710301/311 14-02-2002 dr.ir. A.R.. Koelewijn. ir. J. Lindenberg. 38p.

Erosie kern Diefdijk bij overslag. ir. M.O. de Groot. Deltares report 376270-0000 (2006)

Comcoast report Haskoning (2007) Erosion Tests Sea Dyke report nr. 9R9112.B0/R/401070/Nijm Final Report 21 September 2007 Workpackage 3: Development of Alternative Overtopping-Resistant Sea Defences
Phase 3: Wave Overtopping Erosion Tests at Groningen Sea Dyke

MinIenM 2012. Handreiking Toetsen Grasbekledingen op Dijken t.b.v. de onderbouwing van het beheerdersoordeel (BO) in de derde verlengde toetsronde. Ministerie van Infrastructuur en Milieu. 25-10-2012

K.M. Robinson (1992). Predicting stress and pressure at an overfall. Transactions ASAE 35:2:561-569

K.M. Robinson. G. J. Hanson (1994). A deterministic headcut advance model. Transactions ASAE 37:5:1437-1443.

G. J. Hanson. K. R. Cook. and A. Simon (1999). Determining Erosion Resistance of Cohesive Materials. Int. Water Resources Eng Conf. Seattle. august 1999.

G. J. Hanson. K. M. Robinson. K. R. Cook (2001) Prediction of headcut migration using a deterministic approach. Transactions of the ASAE Vol. 44(3): 525–531 2001 American Society of Agricultural Engineers *ddr.nal.usda.gov/bitstream/10113/26648/1/IND23279974.pdf*

G.J. Hanson. K.R. Cook (2004). Determination of material rate parameters for headcut migration of compacted earthen materials. Proc. of Dam Safety 2004. ASDSO Phoenix. Arizona 2004.

NRCS 1997 National Engineering Handbook part 628 Dams. chapter 51 Earth Spillway Erosion Model and Chapter 52 Field Procedures Guide for the Headcut Erodability Index. Natural Resources Conservation Service. 210-vi-NEH. August 1997

Knoeff, J.G., Calle, E.O.F., Indicatie van reststerkte na overloop / overslag, Delft Cluster, projectnummer 02.02.01, rapportnummer 02.02.01.57, 2002.

Hoffmans. G.J.C.M.. Verheij. H.J.. Scour Manual. publisher A.A. Balkema Rotterdam. 1997

Koelewijn. A.R.. Kruse. G.A.M.. Van. M.A.. Overloop- en bresgroeiproef Proefvak Bergambacht. Delft Cluster 2002. 710301 311.3

List of symbols

c_u	undrained shear strength (kPa)
ϕ'	effective angle of internal friction (^{o})
q_a	average wave overtopping discharge (m^3/s/'m) or (l/s/m)
q	average overtopping discharge (m^3/s/m) or (l/s/m)
q_i	momentary overtopping discharge during the i^{th} overtopping event (m^3/s/m') or (l/s/m)
$q_{i,max}$	maximum overtopping discharge during the i^{th} overtopping event (m^3/s/m') or (l/s/m)
V_i	(individual) wave overtopping volume (m^3/m')
t_i	i^{th} overtopping event duration (s)
t	time (s)
T	time during wave overtopping event when τ_c exceeds τ_e (s)
u_i	momentary depth averaged flow velocity during the i^{th} overtopping event (m/s)
$u_{i,max}$	maximum depth averaged flow velocity during the i^{th} overtopping event (m/s)
u_0	stationary flow velocity on slope (m/s)
$u_{bi\ kr}$	stationary flow velocity on landward side crest (m/s)
h_i	momentary water layer thickness during the i^{th} overtopping event (m)
$h_{i,max}$	maximum water layer thickness during the i^{th} overtopping event (m)
h_0	stationary water layer thickness on slope (m)
$h_{bi\ kr}$	stationary water layer thickness on landward side crest (m)
H	cliff height c.q. scarp height (m)
dX/dt	upstream migration rate (m/s)
$d\varepsilon/dt$	deepening rate (m/s)
k_d	deepening rate parameter c.q. detachment rate coefficient (m/hr/Pa)
τ_c	critical (threshhold) shear stress (Pa)
τ_e	effective shear stress (Pa)
$\tau_{e,i,max}$	maximum effective shear stress during overtopping wave i of N waves (Pa)
τ	shear stress between the overflow and the soil surface (Pa)
κ	constant of Von Kármán (=0.4) (-)
k_s	Nikuradse roughness (m)
D_{90}	Particle diameter
i	slope inclination (m/m)
C_A	Chezy coefficient ()
γ	soil weight (N/m^3)
γ_w	water weight (N/m^3)
$c_{\%}$	clay percentage fraction (-)
C	head cut advance rate coefficient ($s^{-2/3}$)
C_A	Chezy (Antoine de) coefficient ($m^{1/2}$/s)
g	gravitational acceleration (m/s^2)
ρ	specific mass (kg/m^3)
A	head cut advance rate load parameter, $=(qH)^{1/3}$ ($ms^{-1/3}$)
A_0	head cut advance rate threshold parameter ($ms^{-1/3}$)
$A_{i,max}$	maximum head cut advance load during i^{th} overtopping event ($ms^{-1/3}$)
K_h	headcut advance parameter (-)
H_{m0}	$zero^{th}$ moment of the wave height variance spectrum (m)
T_p	peak wave period (s)
T_m	average wave period (s)
N	number of overtopping waves during a considered storm condition (-)
P_{ov}	probability of overtopping of an individual wave reaching the dike (-)

A Parameters from NRCS 1997 chapter 51 and 52

Shields Figure 51-1 estimate of critical sheer stress.

Figure 51–1 Critical stress for incipient motion computed from Shields' criteria with a sediment specific gravity of 2.65 and a kinematic viscosity of water of 10^{-5} ft^2/s

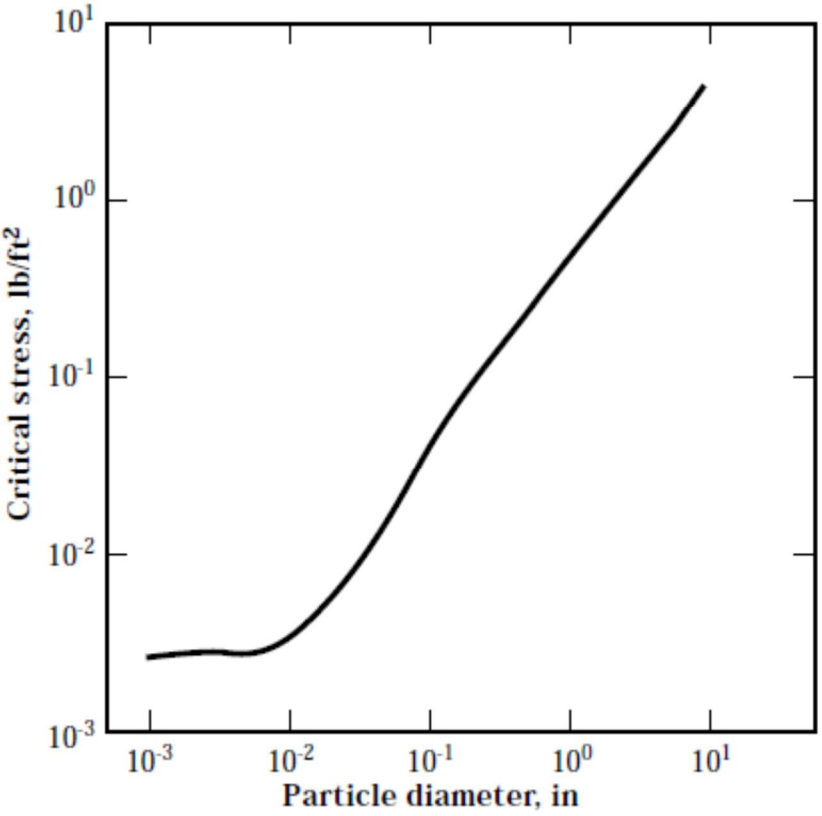

Estimation of M_s.

Table 52–3 Material strength number, M_s, for cohesive soil

Consistency	Field identification tests	SPT (blows/0.3 m)	Unconfined compressive strength (UCS) (kPa)	M_s
Very soft	Exudes between fingers when squeezed in hand.	< 2	< 40	< 0.02
Soft	Easily molded with fingers. Point of geologic pick easily pushed into shaft of handle.	2 - 4	40 - 80	0.02 - 0.05
Firm	Penetrated several centimeters by thumb with moderate pressure. Molded by fingers with some pressure.	4 - 8	80 - 150	0.05 - 0.10
Stiff	Indented by thumb with great effort. Point of geologic pick can be pushed in up to 1 centimeter. Very difficult to mold with fingers. Just penetrated with hand spade.	8 - 15	150 - 300	0.10 - 0.20
Very stiff	Indented only by thumbnail. Slight indentation by pushing point of geologic pick. Requires hand pick for excavation.	15 - 30	300 - 625	0.20 - 0.45

Notes:
1. Cohesive soil is material with a plasticity index (PI) greater than 10. Use table 52–2 for cohesionless soils.
2. 1 kPa equals 1 kN/m².
3. Vane shear strength (ASTM D 2573, field; ASTM D 4648, lab) also may be used for unconfined compressive strength (ASTM D 2166).
4. Cohesive soils in which blow counts are greater than 30 or strengths greater than 625 kPa are to be taken as rock, for which the hardness can be obtained from table 52–4.
5. Cohesive soils must be evaluated for hardness in the saturated condition.
6. M_s of a cohesive soil also can be determined as the product of unconfined compressive strength (in MPa) times its coefficient of relative density. For most cohesive soils, M_s is approximately determined by:

   $M_s = 0.78\ (UCS)^{1.09}$ for UCS ≤ 10 MPa, and M_s = UCS for UCS > 10 MPa.
7. Correlation between SPT and UCS should only be used as a guide, as results may vary in geologic areas. Lab strength tests are recommended on soil materials to support SPT or field assessment tests. Vane shear strength values also are applicable in the lower strength ranges.

Estimation of K_b. Page 52-8 from NRCS 1997

(b) Block/particle size number (K_b)

The term K_b represents the mean size of individual material units as determined by the spacing of discontinuities in a rock mass, or it is a function of particle diameter of cohesionless granular soils, including detritus and boulder formations. The number can be calculated by a variety of approaches.

(2) Cohesive soils and coarse detritus, gravels, and boulders

For intact, cohesive soils and coarse detritus, gravels, and boulder formations for which D > 0.1 meter, $K_b = 1$. For strongly cemented materials that lack discontinuities, RQD = 100 and $J_n = 1$. If soil joints occur within the soil mass, use equation 52–3 to obtain RQD and apply the applicable value for J_n to obtain K_b by equation 52–2.

Whether material units erode as individual constituent particles or by blocks of material depends on the occurrence of discontinuities within the mass. In rock formations, only discontinuities that effectively break the mass into discrete blocks are to be considered.

Estimation of K_d.

(2) Interparticle bond shear strength

If the material under consideration occurs as a soil mass or as gouge in the apertures of rock discontinuities, the interparticle bond shear strength number, K_d,

---

is represented by the quotient J_r/J_a, that, in turn, is approximately equal to tan ϕ'_r, where ϕ'_r is the residual (minimum) friction angle. The residual friction angle can be estimated according to a relationship with soil index properties (Stark and Eid, 1994).

Figure 52–1 presents a correlation of drained residual friction angle (ϕ'_r) and liquid limit (LL) for shear tests conducted on cohesive clays at an effective normal stress of 100 kPa, a value considered typical of near surface materials. The data form three distinct curves according to three ranges of clay size fraction:

For ≤ 20% clay, $\phi'_r = 169.58\ (LL)^{-0.4925}$ [52–7]

For 25 – 45% clay, $\phi'_r = 329.56\ (LL)^{-0.7100}$ [52–8]

For ≥ 50 % clay, $\phi'_r = 234.73\ (LL)^{-0.6655}$ [52–9]

The interparticle bond shear strength number (K_d) of a cohesive soil is predicted by a rational correlation between soil index properties and residual shear strength by the following method (Moore, 2001).

1. Determine the liquid limit by ASTM D 4318, Standard Test Method for Liquid Limit, Plastic Limit, and Plasticity Index of Soils, and report the result to the nearest one percent.
2. Determine clay content (the percent finer than 0.002 mm) by ASTM D 422, Standard Test Method for Particle-Size Analysis of Soils, and report the result to the nearest five percent.
3. Use the clay content value to select the appropriate equation (52–7, 52–8, or 52–9) to predict effective residual friction angle, ϕ'_r, and report the result to the nearest one-tenth degree.

Typical ranges of friction angles for various materials are provided in table 52–9. If the residual friction angle calculated by this method differs significantly from these values, consider conducting laboratory or in situ standard test methods, such as:

- ASTM D 3080, Direct Shear Test of Soils Under Consolidated Drained Conditions
- ASTM D 6467, Torsional Ring Shear Test to Determine Drained Residual Shear strength of Cohesive Soils

Once the friction angle is determined, the interparticle bond shear strength number, K_d, is determined by

$$K_d \cong \tan \phi'_r \qquad [52\text{-}10]$$

Estimation of J_s. Page 52-12/13 from NRCS 1997

(d) Relative ground structure number

The relative ground structure number (J_s) represents the orientation of the effective dip of the least favorable discontinuity with respect to spillway flow. The number takes into account the effect of the relative shape of the material units (as determined by joint set spacings) or the ease with which the spillway flow penetrates the ground and dislodges individual material particles.

For practical expediency the rock mass is assumed to be intersected by two primary joint sets in the plane at right angles to spillway flow. The value of J_s is expressed in terms of the relative spacing of the two

Table 52–11 Weathering condition of joint face material

Descriptor	Weathering condition of joint face material
Fresh	No sign of weathering.
Discolored	Iron-stained or discolored, but otherwise unweathered.
Disintegrated	Physically disintegrated to a soil condition with original fabric still intact; material is friable; mineral grains are not decomposed.
Decomposed	Chemically altered to a soil condition with original fabric still intact; some or all of mineral grains are decomposed.

joint sets, the dip angle and the dip direction of the closer spaced set relative to the direction of spillway flow. In this methodology, soil material is considered intact (without structure), in which case $J_s = 1$.

B Critical velocity and critical bed shear stress cohesive soils

In the Scour Manual (Hoffmans and Verheij. 1997) rough estimates are given for the critical depth averaged flow velocity U_c (m/s) for cohesive soils based on qualitative descriptions of the clay content and compaction (Table B.1).

Table 2.4. Critical depth-averaged velocities for cohesive sediments (rough estimates).

Type of soil	h (m)	U_c (m/s)
Loamy sand, light loamy clay with low compactness	1	0.4
Heavy loamy clay with low density	3	0.5
Low density clay	10	0.6
Light loamy clay with medium compactness	1	0.8
Heavy loamy clay with medium density	3	1.0
Clay of medium density	10	1.3
Light loamy clay (dense)	1	1.2
Heavy loamy clay (dense)	3	1.5
Hard clay	10	1.9

Table B.1 Rough estimates for U_c (m/s) for different cohesive materials and compaction (Hoffmans and Verheij 1997)

In the same Scour Manual a formula based on experiments by Mirtskhoulava is given. where the critical velocity depends on the soil fatigue rupture strength c_f (Pa). volumetric mass of the erodible particles ρ_s (kg/m^3) and the erodible aggregate diameter d_a (m). The fatigue rupture strength is related to the cohesion c_0 (pa); c_f=0.035*c_0. Values of c_0 as a function of the liquidity index Ic (-) and the void ratio e (-) are suggested in the scour manual (Table B.2).

Table 2.5. C_o in kPa and ϕ' in degrees (given in brackets); rough estimates (Mirtskhoulava 1988).

Type of soil and range of liquidity index	Soil property at voids ratio						
	0.45	0.45	0.65	0.75	0.85	0.95	1.05
Loamy sand							
0-0.25	14.7	10.8	7.85				
	(30)	(29)	(27)				
0.25-0.75	12.7	8.83	5.88	2.94			
	(28)	(26)	(24)	(21)			
Loamy clay							
0-0.25 (low plasticity)	46.1	36.3	30.4	24.5	21.6	18.6	
	(26)	(25)	(24)	(23)	(22)	(20)	
0.25-0.5 (medium plasticity)	38.2	33.3	27.5	22.6	17.7	14.7	
	(24)	(23)	(22)	(21)	(19)	(17)	
0.5-0.75 (high plasticity)			24.5	19.6	15.7	13.7	11.8
			(19)	(18)	(16)	(14)	(12)
Clay							
0-0.25		79.4	66.8	53.0	46.1	40.2	35.3
		(21)	(20)	(19)	(18)	(16)	(14)
0.25-0.5			55.9	49.0	42.2	36.3	31.4
			(18)	(17)	(16)	(14)	(11)
0.5-0.75			44.1	40.2	35.3	32.4	28.4
			(15)	(14)	(12)	(10)	(7)

in which: $C_f = 0.035 C_o$ Pa (1 Pa = 1 N/m²), fatigue rupture strength of clay,
C_o is cohesion (Table 2.5)
d_a = size of detaching aggregates, $d_a = 0.004$ m
h = flow depth (m)
U_c = critical mean velocity for cohesive sediments (m/s)

Based on the work of Mirtskhoulava (1988, 1991), a simplified expression for the critical depth-averaged velocity for cohesive sediments is:

$$U_c = \log\left(\frac{8.8h}{d_a}\right)\sqrt{\frac{0.4}{\rho}\left((\rho_s - \rho)gd_a + 0.6C_f\right)} \qquad (2.9)$$

Table B.2 Rough estimates of c_0 (kPa) for different values of the liquidity index and void ratio for cohesive soils and the relation between U_c (m/s) and soil parameters by Mirtskhoulava (Hoffmans and Verheij 1997).

Entering a water depth of h=1 m in the formula. d_a= 4 mm. ρ_{soil} based on the void ratio and a grain mass density of 2650 kg/m^3. the following critical velocities are calculated (Table B.3).

U_c (m/s)	Loamy clay			Clay		
n (-)	Ic=0-0.25	Ic=0.25-0.5	Ic=0.5-0.75	Ic=0-0.25	Ic=0.25-0.5	Ic=0.5-0.75
0.31	2.10	1.92				
0.35	1.87	1.80		2.75		
0.39	1.72	1.64	1.55	2.53	2.32	2.06
0.43	1.56	1.50	1.40	2.26	2.17	1.97
0.46	1.47	1.34	1.27	2.11	2.02	1.86
0.49	1.37	1.23	1.19	1.98	1.88	1.78
0.51			1.12	1.86	1.76	1.68

Table B.3 U_c (m/s) from formula Mirtskhoulava (Hoffmans. Verheij 1997) where d_a=0.004 m and h=1 m. for different values of the porosity n (-) and liquidity index Ic (-)

The calculated critical velocities are slightly higher than the values given in Table B.1 for h=1 m. For wave overtopping conditions the water layer thickness varies from a few centimetres up to ca. 0.3 m the critical velocity will be lower (see Table B.4 for a value of h=0.1 m).

U_c (m/s)	Loamy clay			Clay		
n (-)	Ic=0-0.25	Ic=0.25-0.5	Ic=0.5-0.75	Ic=0-0.25	Ic=0.25-0.5	Ic=0.5-0.75
0.31	1.47	1.34				
0.35	1.31	1.26		1.93		
0.39	1.21	1.15	1.09	1.77	1.62	1.45
0.43	1.09	1.05	0.98	1.58	1.52	1.38
0.46	1.03	0.94	0.89	1.48	1.42	1.30
0.49	0.96	0.86	0.84	1.39	1.32	1.25
0.51			0.79	1.30	1.23	1.18

Table B.4 U_c (m/s) from formula Mirtskhoulava (Hoffmans. Verheij 1997) where d_a=0.004 m and h=0.1 m. for different values of the porosity n (-) and liquidity index Ic (-)

The parameters of cohesion. particle weight and diameter are uncertain. difficult to measure and depend on local circumstances and material properties. The given critical velocities are just as stated in the manual 'rough estimates'. The order of magnitude of the critical velocity for different cohesive soils is however captured in the given tables.

Some erosion formulae require the critical bed shear stress τ_c (Pa) to determine the hydraulic load at the start particle motion. Both parameters are related. combining:

$$\tau_c = \rho U_{*,c}^2$$

$$U_c = U_{*,c} \frac{C}{\sqrt{g}}$$

results in:

$$\tau_c = \frac{\rho g}{C^2} U_c^2$$

Where C ($m^{0.5}$/s) is the Chézy coefficient. For grass slopes in wave overtopping conditions the coefficient is in the order of 25-30 $m^{0.5}$/s. C can also be expressed in terms of the equivalent roughness of Nikuradse (m) and the hydraulic radius R (m):

$$C = \frac{\sqrt{g}}{\kappa} \ln\left(\frac{12R}{k_s}\right)$$

κ is the von Kármán 0.4 (-). For wave overtopping conditions the hydraulic radius can be approximated by the water layer thickness. For hydraulic rough flow. which applies for wave overtopping conditions. the Nikuradse equivalent roughness on a granular surface can be approximated by $k_s=3*d_{90}$ (Hoffmans and Verheij 1997). For example if the water layer thickness is 0.1 m and the grass has a roughness 'd_{90}' in the order or 0.02 m C = 23 $m^{0.5}$/s. For the range of critical velocities in Table B.4 and the estimated Chézy coefficient the formula results in the τ_c's given in Table B.5.

τ_c (Pa)	Loamy clay			Clay		
n (-)	I_l=0-0.25	I_l=0.25-0.5	I_l=0.5-0.75	I_l=0-0.25	I_l=0.25-0.5	I_l=0.5-0.75
0.31	40.2	33.5				
0.35	32.0	29.4		68.8		
0.39	27.0	24.5	22.0	58.1	48.8	38.7
0.43	22.1	20.4	17.9	46.4	43.0	35.5
0.46	19.7	16.3	14.6	40.6	37.3	31.4
0.49	17.2	13.8	13.0	35.6	32.3	29.0
0.51			11.4	31.5	28.2	25.6

Table B.5 τ_c (Pa) based on U_c (m/s) from Table B.4 and C=23 $m^{0.5}$/s; R=h=0.1 m. $k_s=3*'d_{90}'=0.06$ m.

The given critical bed shear stress are a rough estimate.

C Literature on model developments head cut migration

In section 5 the empirical model from NRCS is described with which the head cut migration and deepening was calculated for two cases and more in general (section 6). The models were found to be most suitable for this study. The rate factors in the empirical formulae have been subject to development in a more deterministic way. These developments were considered not to have more value for this limited study, but are considered to be promising for further studies and are therefore described in this Appendix.

C.1 The deterministic headcut migration analysis

Hanson, Robinson and Cook (2001) developed a deterministic approach to headcut migration, which they describe in the following terms:

> "Robinson and Hanson (1994) developed a deterministic physically based model to predict headcut advance that assumed headcut migration by undercutting and vertical headwall failure. This model predicts headcut failure by erosion of the headcut face and the downstream channel due to hydraulic stresses in the plunge pool region of the headcut. The model includes a soil strength component for prediction of headcut failure and underlying assumptions related to debris clean out downstream of the headcut. The rate of headcut migration is based on measurable input parameters of soil strength, soil unit weight, erodibility and critical shear stress, initial overfall height, depth to a more erosion–resistant layer, backwater level, and discharge."

The method is of great interest, because it is a step in the right direction away from purely empirical methods. It uses a sensible and simple model of headcut development, and appears to fit flume test data well. This approach is considered promising for application to the case of overtopping after inner dyke slope failure, because it starts from an already formed headcut (Figure C.1 and Figure C.2).

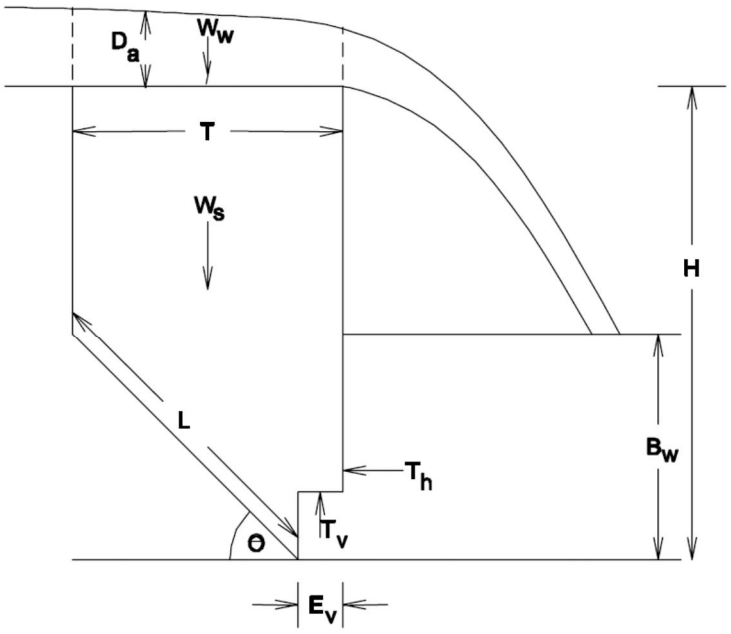

Figure 1. Overfall forces (Robinson and Hanson, 1994).

Figure C.1 Overfall forces from Robinson and Hanson, 1994

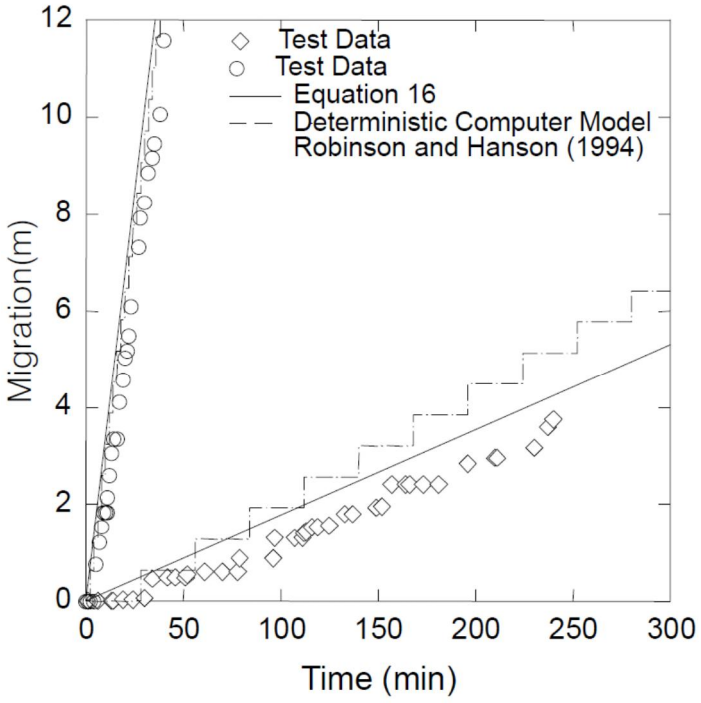

Figure 4. Measured and predicted headcut migration for two flume tests.

Figure C.2 Measured and predicted headcut migration time (min) vs migration (m) from Hanson, Robinson and Cook (2001), which also holds 'Equation 16'

A vertical headcut H is subject to overflow, and is gradually undercut by erosion at the toe. When erosion depth E_v has progressed sufficiently, the combined increase of uplift and the reduction in length of shear surface lead to slip failure for which the Culman analysis is assumed. The soil strength is represented by c_u. A migration rate is derived from T/t_f where T

is the distance from the headcut to the tension crack behind the face, and t_f is the time needed for E_v to develop to the stage that failure occurs. A simple adaption of the wasting formula of erosion in Phase 1 and 2 analyses results:

$$\frac{dX}{dt} = \left(\frac{H}{2E_v} \right) k_d \, (\tau_e - \tau_c)$$

Values for the factor ($H/2E_v$) are determined from the flume tests. Values higher than 1 point to failure occurring before the undercutting has reached the tension crack. This factor appears to be dependent on the ratio of backwater depth to total headcut height: a larger depth of a plunge pool at the toe of the headcut allows deeper undercutting to develop before failure occurs (Figure C.3).

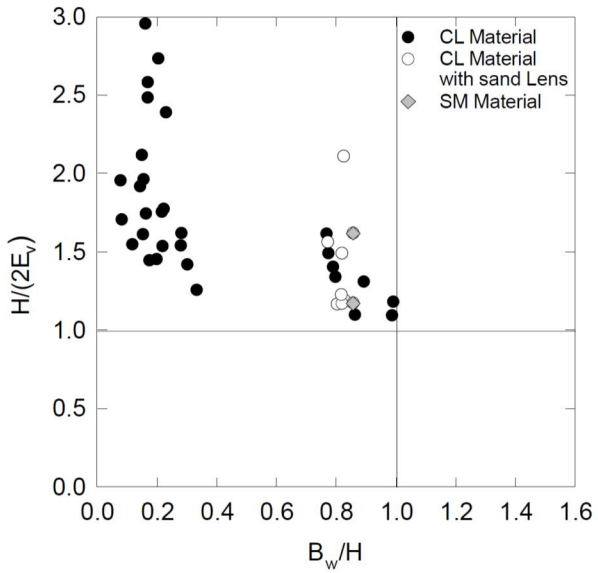

Figure 6. Variation of $H/(2E_v)$ versus B_w/H.

Figure C.3 Factor $H/(2E_v)$ (-) vs B_w/H (-) Figure 6 from Hanson, Robinson and Cook (2001)

Methods are mentioned to determine k_d and τ_c from jet erosion tests, and the effective shear stress τ_e in the undercut is predicted by dimensionless equations developed in earlier work by Robinson (1992).

(Note that these authors reserve the words "stress" for the geotechnical term shear stress and "pressure" for fluid stress.)

A specific boundary condition is imposed by the flume: downwards erosion is limited by the flume floor.

The case of overtopping after inner slope failure also has a pre-existing "headcut" or scarp, and the height applied in Hanson's flume tests was 0.9 to 1.5 m, while scarp heights are typically 0.5 to 1.0 m, and is limited in its downward erosion by the grass cover, (or in the case of a crest slip through an existing road, the asphalt cover) just as in the flume it is by the floor. The model requires as parameters the offset-linear erosion model parameters k_d and τ_C

and the soil strength c_u and density. Geometric parameters are headcut or scarp height, depth of water above (nappe) and below (backwater).

The strength c_u determines E_v. For simplicity, the factor $H/2E_v$ could be set at a conservative value of say 3.5. This would be sufficient to establish the overly safe cases of overtopping, with obviously large reserves against headcut advance. Then only the erosion parameters and shear stress are needed.

The equations given by Robinson (1992) from which the shear stresses can be calculated are given in the following. In the derivation, it was assumed that the nappe was not aerated. This brings the nappe closer to the vertical face, and increases shear stress. The author warns that the solutions are only applicable to velocities such that Froude's number at the brink is higher than 1, which will be the case for most wave overtopping situations.

Horizontal Stress Magnitude. The magnitude of the maximum time-averaged horizontal stress (τ_h) can be represented as:

$\pi_1 = \tau_h/(\gamma D_a)$
γ = unit weight of the water
$\pi_2 = q^2/(g D_a^3)$
$\pi_3 = H/D_a$
$\pi_4 = B_w/D_a$

Again considering only plunging nappes ($B_w \leq 0.9$ H), the stress prediction equations for high and low backwater cases are:

$$\pi_1 = 0.032\ \pi_2^{0.204}\ \pi_3^{0.852}\ \pi_4^{-1.796} \quad \text{(High Backwater)} \quad (9)$$

$$\pi_1 = 0.011\ \pi_2^{-0.001}\ \pi_3^{0.582}\ \pi_4^{-0.114} \quad \text{(Low Backwater)} \quad (10)$$

Horizontal Stress Location.

$$X_h = D_s + 1.417\ D_a$$

Vertical Wall Stress Magnitude. The magnitude of the maximum stress on the vertical wall (τ_v) can be represented as:

$\pi_1 = \tau_v(\gamma D_a)$
$\pi_2 = q^2/(g D_a^3)$
$\pi_3 = H/D_a$
$\pi_4 = B_w/D_a$
$\pi_5 = X_p/D_a$

X_p is the location of the maximum pressure on the horizontal floor, and γ is the unit weight of the water.

$$\pi_1 = 0.025\ \pi_2^{-1.295}\ \pi_3^{0.026}\ \pi_4^{0.221}\ \pi_5^{-1.062} \qquad (12)$$

Horizontal Stagnation Pressure Location.

$$\frac{S}{N_l} = 0.154\ \mathrm{COT}\ (A_n) \qquad (7)$$

where S represents eccentricity, per Schauer and Eustis (1963).

$$X_p = D_s - S - \left(\frac{N_w}{2}\right) \qquad (8)$$

C.2 Adaption of headcut erosion model to overtopping on failed inner slope scarp

The headcut erosion model of Hanson, Robinson and Cook (2001) is adapted slightly to fit the case of overtopping flow over the scarp of an inner dyke slope slip failure. The figure below is referred to.

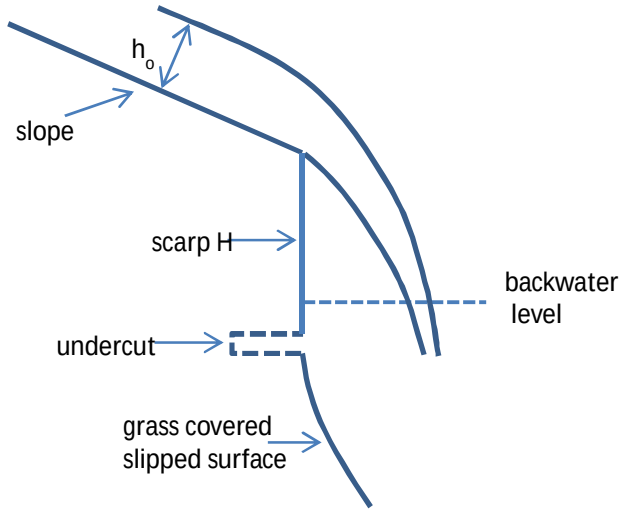

Figure C.4 Slightly adapted headcut erosion model of Hanson, Robinson and Cook (2001) for the case of overtopping flow over the scarp of an inner dyke slope slip failure

The adaptation and assumptions are the following:

- The nappe (Dutch: het vlak van het overstortende water) profile is taken from Robinson (1992). The angle of the slope above the headcut, not existent in the original model, is accounted for by finding that point on the lower nappe profile where the nappe angle equals the upper slope angle. This results in a correction (upwards) to the scarp height, to obtain the equivalent headcut height with overfall from a horizontal approach surface
  Note: the slope of the lower nappe at the brink probably is steeper than the approach slope due to the effect of gravity. The more so for lower Froude numbers. Accounting for this would increase shear stress on the vertical wall.
- flow over the approach surface follows from the Chezy and Manning equations
- vertical thickness of the nappe is constant.
- The grass covered slipped surface at the bottom of the scarp is taken to be horizontal, as in the model, even though it is usually quite steep.
- The backwaterlevel is taken to maximise shear stress on the scarp.

The depth h_o is the free flowing depth along the approach surface. With a horizontal approach surface, the vertical nappe depth or brink depth is 0.714 x the critical depth and the latter occurs 3 to 4 x the critical depth back from the brink. Here it is assumed that the enhanced gravity component at the initiation of the nappe due to the inclined approach surface, reduces the difference, and for simplicity, nappe depth is taken as h_o. This assumption results in a reduction to approx. 0.90 x critical depth at the brink ($h_0 \times \sqrt{(1+i^2)}$ to h_0). An adapted Rouse derivation for overfall from an inclined surface is needed to find the correct value.

The overfall height reduces when account is taken of the inclination of the approach slope. The adjustment is however very minimal, and the overfall height needed in the calculations of

the model is only very slightly higher than the actual scarp height. For simplicity, both heights are taken equal.

Robinson (1992) gives the following expression for the maximum shear stress on the vertical face:

$$\frac{\tau_v}{\gamma D_a} = 0.025\left(\frac{q^2}{gD_a^3}\right)^{-1.295}\left(\frac{H}{D_a}\right)^{0.026}\left(\frac{B_w}{D_a}\right)^{0.221}\left(\frac{X_p}{D_a}\right)^{-1.062}$$

and for the maximum shear stress at the bottom of the plunge pool:

$$\frac{\tau_h}{\gamma D_a} = 0.032\left(\frac{q^2}{gD_a^3}\right)^{0.204}\left(\frac{H}{D_a}\right)^{0.852}\left(\frac{B_w}{D_a}\right)^{-1.796}$$ for high backwater levels, and

$$\frac{\tau_h}{\gamma D_a} = 0.011\left(\frac{q^2}{gD_a^3}\right)^{-0.001}\left(\frac{H}{D_a}\right)^{0.582}\left(\frac{B_w}{D_a}\right)^{-0.114}$$ for low backwater levels.

Obviously, no shear stress is present on the vertical face if backwater is absent. It also attenuates quickly as the distance X_p to the location of the maximum shear stress at the bottom of the plunge pool increases.

Figure C.5 shows a result of the adapted model. The nappe as given by Robinson is taken up from the point its lower inclination equals the slope inclination, taken here as i = -0.5. See the dashed brown or orange line.

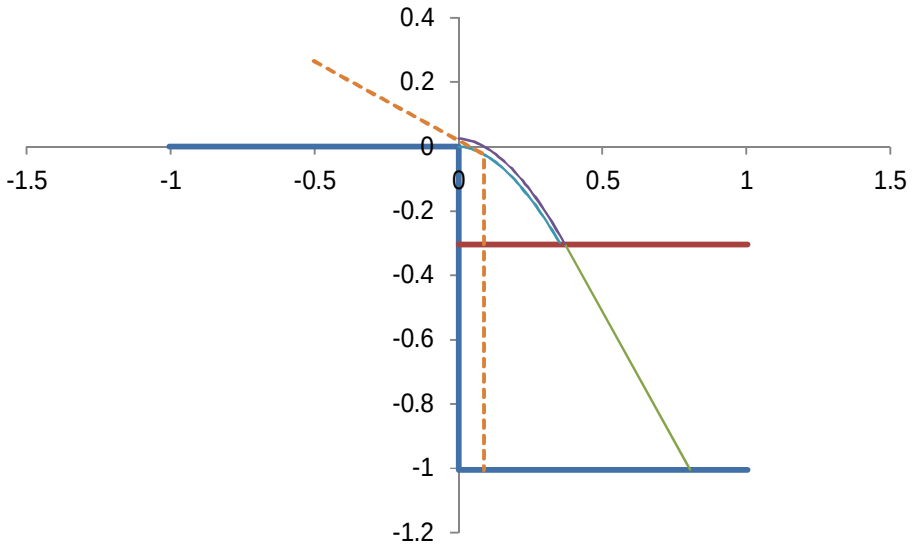

Figure C.5 Result of the adapted model

The thickness of the nappe follows from the flow on the grass covered approach slope, for which a Manning coefficient of 0.03 was used. The discharge was 50 liter/m/s, and the backwater depth was chosen to maximise τ_v. A very thin nappe is found of only 2.5 cm thick, with a Froude number at the brink of 3.7. The jet shoots out very far due to its high velocity,

and so the shear stress on the vertical face is very small, only 0.036 kPa. The maximum shear stress on the bottom of the plunge pool is 1.05 kPa in this case.

Although low shear stresses are found in the present case, the free overfall model together with the deterministic approach to headcut advance seem plausible, and are possibly useful for the case of scarp erosion, both at the crest and on the slope. The necessity of a backwater depth to obtain any shear stress on the vertical face at all is not necessarily a drawback. Overshooting nappes may well occur in practice, and the focus should then be on the impact shear stresses at the base of the nappe. Unluckily, Robinson's equations do not apply to this case, as τ_h tends to infinity if B_w approaches zero. Further, the sloping run-off surface below the headcut will also modify both the impact stresses as well as the geotechnical stability equations of the headcut.

The model merits more consideration and adaptation, to obtain a sensible alternative to the present simple but empirical equations.